

MRI insight on natural methane hydrate reservoir system with hydrate, water and gas layers: Development basis of higher-pressure gas reservoir under hydrate layer

Guojun Zhao¹, Huiru Sun¹, Mingjun Yang¹, Jia-nan Zheng¹, Xin Lv², and Yongchen Song¹

¹Dalian University of Technology

²China National Offshore Oil Corporation

November 22, 2022

Abstract

High-pressure methane gas generally exists stably under methane hydrate stability zone at several hundred meters cutting through the marine sedimentary strata. The usually employed bottom simulating reflector (BSR) for hydrate recognition represents the interface between hydrate and fluid areas in typical natural methane hydrate reservoir system with hydrate, water and gas layers. In this study, the gas-seawater migration in hydrate reservoir was simulated through gas-seawater injection, and the existence of hydrate-containing sealing layer was experimentally confirmed. The hydrate reformation was observed by MRI during the gas-water injection process above the methane hydrate phase equilibrium pressure and it is the fundamental reason that hydrate reservoir has sealing effect on free gas. As the decrease of pore spaces in sediments, the interaction of seawater and hydrate in the reservoir products capillary sealing in the narrow space, thus the free gas and seawater migration are inhibited and the free gas existed stably underlying the hydrate layer. However, low methane concentration in seawater caused by high gas-water flow rate (4-1 ml/min) resulted in the hydrate dissociation, the hydrate-bearing sediments can't produce the sealing effect. Hydrate further forms in the sealing layer and leads to seawater depletion until it is too salty to form hydrate. Finally, the gas layer, water layer and hydrate layer coexist under the seabed. In addition, the hydrate-containing sealing layer could be broken through, and the breakthrough pressure is a significant parameter for hydrate reservoir.

MRI insight on natural methane hydrate reservoir system with hydrate, water and gas layers: Development basis of higher-pressure gas reservoir under hydrate layer

Guojun Zhao¹, Huiru Sun¹, Mingjun Yang¹, Jia-nan Zheng¹,^{11*} Corresponding authors. *E-mail addresses* : zhengjn@dlut.edu.cn (**J. Zheng**) and songyc@dlut.edu.cn (**Y. Song**), Xin Lv², Yongchen Song^{1,*}

¹ *Key Laboratory of Ocean Energy Utilization and Energy Conservation of Ministry of Education, Dalian University of Technology, Dalian 116024, China*

² *CNOOC Research Institute Co. Ltd, Beijing 100027, China*

Key points:

* First-time experimental visualization on the theoretic sealing effect of natural gas hydrate on its lower gas by MRI.

* Further formation or dissociation of initial formed hydrate under excess water is critical to whether the sealing effect works.

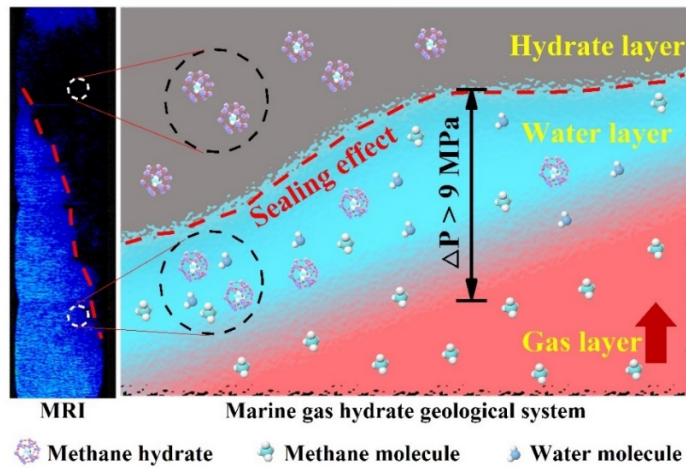
* At least 9.0 MPa pressure difference can exist on both sides of the manmade methane hydrate-containing sealing layer.

Abstract :High-pressure methane gas generally exists stably under methane hydrate stability zone at several hundred meters cutting through the marine sedimentary strata. The usually employed bottom simulating reflector (BSR) for hydrate recognition represents the interface between hydrate and fluid areas in typical natural methane hydrate reservoir system with hydrate, water and gas layers. In this study, the gas-seawater migration in hydrate reservoir was simulated through gas-seawater injection, and the existence of hydrate-containing sealing layer was experimentally confirmed. The hydrate reformation was observed by magnetic resonance imaging (MRI) during the gas-water injection process above the methane hydrate phase equilibrium pressure and it is the fundamental reason that hydrate reservoir has sealing effect on free gas. As the decrease of pore spaces in sediments, the interaction of seawater and hydrate in the reservoir products capillary sealing in the narrow space, thus the free gas and seawater migration are inhibited and the free gas exited stably underlying the hydrate layer. However, low methane concentration in seawater caused by high gas-water flow rate (4–1 ml/min) resulted in the hydrate dissociation, the hydrate-bearing sediments can't produce the sealing effect. Hydrate further forms in the sealing layer and leads to seawater depletion until it is too salty to form hydrate. Finally, the gas layer, water layer and hydrate layer coexist under the seabed. In addition, the hydrate-containing sealing layer could be broken through, and the breakthrough pressure is a significant parameter for hydrate reservoir.

Keywords: Natural hydrate reservoir; Sealing effect; Gas-water flow; MRI

Plain Language Summary

Typical methane hydrate reservoir system in nature generally includes hydrate, water and gas layers, and the already explored marine hydrate reservoir (recognized by bottom simulating reflector method) is just corresponding to this geological reservoir distribution. In marine geology, real gas layer existing stably under the hydrate and water layers may be with higher pressure because of the sealing effect of hydrate layer, and the accurate pressure condition of fully developed gas layer is rarely investigated. We confirm this assumption of natural hydrate and gas reservoirs system accumulation and obtain an entire image of the typical system visually by magnetic resonance imaging. We find that the sealing effect is mainly due to the hydrate reformation and liquid water residue. In order to evaluate the mechanical stability of the sealing effect, we increase the gas pressure to 13 MPa and verify the permitted pressure difference between the two sides of the sealing layer higher than 9.0 MPa. Future geological exploration and joint exploitation project of hydrate and gas reservoirs should refer to these results.



TOC graphic:

Introduction

Vast quantities of energy that mankind craves hidden at the bottom of ocean, natural gas hydrate (NGH) is a representative one (Huang *et al.* , 2011). NGH only form under low temperature and high pressure area with sufficient gas and water (Zhong *et al.* , 2016). Seismic reflection method is one the most effective method to detect marine gas hydrate (Tian and Liu , 2020). There are two chief kinds of seismic waves: body waves and surface waves, body waves are mainly used in geological survey. Body waves are divided into longitudinal waves (P waves) and shear waves (S waves). For hydrate in sediments, S waves are more sensitive than P waves, and seismic surveys take the advantage of this acoustic property to detect NGH (Helgerud *et al.* , 2011). The bottom simulating reflector (BSR) on seismic profile is considered the mark of interface between gas hydrate area and free gas area. Above the BSR, the natural gas exists in hydrate form, and the natural gas exists in the form of free gas below (Petersen *et al.* , 2007). Well logging is another important geophysical method in gas hydrate detect besides seismic reflection, mainly include resistivity log, spontaneous potential log, caliper log, density log and so on (Ning *et al.* , 2013).

According to preliminary statistics, the total amount of stored NGH is approximately $2.1 \times 10^{16} m^3$, nearly twice of the traditional fossil fuel (oil and natural gas) reserves in the world, and the total NGH stored in deep sea sediment is up to 99% (Makogon , 2010). In the South China Sea, the NGH resourced is up to $(64.35-77.22) \times 10^9$ t of oil equivalent (Liu *et al.* , 2019), amounting to about half of the total resources of onshore and offshore oil and gas in China (Shi *et al.* , 2019). So far, two NGH production test were carried out in China. In 2017, the China Geological Survey conducted the first production test in Shenhu area (Li *et al.* , 2018). From October 2019 to April 2020, the second offshore NGH production test was conducted in 1225 m deep Shenhu Area (Liang *et al.* , 2020). The success of second production test indicates that safe and effective NGH exploitation is feasible in clayey silt NGH reservoirs (Qiang *et al.* , 2020). Meanwhile, multiple techniques have been tested in Shenhu drilling area. The amplitude behaviors of gas hydrate from stacked seismic data were analyzed, the result shown that free gas zone was accompanied below the gas hydrate zone (Pibo *et al.* , 2017). Through detailed logging data and core analysis from 2020 offshore production test, there was a 24.6 m thick layer consisting of hydrate, free gas and water which was below the hydrate layer

(*Qin et al.* , 2020).

Not just in South China Sea, the free gas zone was found stably existed underlain the hydrate reservoir in other areas (*Flemings et al.* , 2003; *Merey and Longinos* , 2018), and it was estimated that the free gas zone may contain from 1/6 to 2/3 of the total methane trapped in hydrate (*Hornbach et al.* , 2004). *Moridis et al.* (2007) also pointed the spatial structure of hydrate reservoir with the free gas and water below the hydrate zone. Recent research had confirmed that in the Hydrate Ridge in offshore Oregon, the hydrate, free gas and seawater coexisted in the hydrate stability zone (*Milkov et al.* , 2004). As for as the Green Canyon in the Gulf in Mexico (*Zhang. and McConnell* , 2010) and the Nankai Trough in Japan (*Miyakawa et al.* , 2014). In 1967, the Messoyakha gas field was discovered in Siberia permafrost, the gas zone was enclosed in an anticlinal tectonic circle, and the top of free gas zone was covered with gas hydrate (*Makogon et al.* , 2005). The impermeable boundary was the sedimentary layer which between the gas hydrate zone and the free gas zone (*Collett and Ginsburg* , 1998). Simulation Study shown that the production intervals should be placed far from the impermeable boundary to attain high gas production rates (*Graver et al.* , 2008).

The mechanism of sealing effect for gas hydrate layer is the capillary force between water and hydrate (*Dillon et al.* , 1980; *Su et al.* , 2009). Early in 1999, *Clennell et al.* (1999) systematically analyzed the effect of capillary pressure on the pore pressure, they explained the pressure of underlying free gas was higher than the theoretical pressure of the formation fluid due to capillary pressure. In recent years, the research of gas hydrates has been gradually developing towards microscopic direction, and the influence of capillary force on gas hydrate has been paid more attention by scholars at home and abroad. *Touil et al.* (*Touil et al.* , 2019) studied the formation of carbon dioxide hydrate in thin glass tube, the capillary force constrained the direction of hydrate growth, and hydrate grow along the front of the glass wall. *Buleiko et al* (2017) found the change of propane hydrate formation pressure in porous media using micro calorimeter, because the thermodynamic properties of propane was changed by the capillary effect of pores, which affected propane hydrate.

The large amount of free gas underling the hydrate-containing sealing layer cannot migrate upward because of the sealing effect of hydrate-containing sealing layer (*Dillon et al.* , 1980). Early, natural gas in the deep ocean floor moved upward mainly through diffusion effect (*Ming et al.* , 2017),and solid hydrate is formed in the sedimentary layer that meets the conditions of hydrate formation during this process. Thus, the porosity of the sediments is significantly reduced. The residual water in the narrow pore space of the sedimentary layer creates capillary forces, which pointed down the free gas layer with larger pores volume. Thereby, the hydrate-containing sealing layer is formed to inhibit the upward migration of underlying gas (*Xu and Ruppel* , 1999).

However, the hydrate-containing sealing layer is not unbreakable. There have been cases of gas leakage under the seabed, such as along the Cascadia continental margin (*Heeschen et al.* , 2005) and offshore Vancouver Island (*He et al.* , 2009). The cold fluids consisting water and hydrocarbon (mostly methane) below the seafloor deposit interface migrate to the seabed by leakage, gushing, or diffusion, this is the cold vent (*Logan et al.* , 2010). The appearance of cold vent is a typical breakthrough of hydrate-containing sealing layer. The gas and seawater generated by breakthrough of hydrate-containing sealing layer will lead to sedimentary layer deformation above the hydrate layer, even cause marine geological disaster (*Yang et al.* , 2020). Therefore, the destruction of hydrate-containing sealing layer must be considered during the hydrate exploitation process.

Although the Marine geology theory has long proposed that hydrate-containing sealing layer is the key for hydrate accumulation, there is no direct experimental evidence of hydrate-containing sealing layer. In this study, the formation process and the existence mode of the hydrate-containing sealing layer were investigated by simulating the process of gas-water migration, the effect of different gas-seawater flow rate and different reservoir pressure on the formation of the hydrate-containing sealing layer was also investigated by MRI. MRI technique was widely used in hydrate investigations because it can distinguish the solid hydrate and liquid water (*Song et al.* , 2015). The research consideration was quit novel, the findings has the significant practical application value to understand the characteristics of hydrate reservoir.

Experimental apparatus and procedure

Apparatus

The experimental apparatus is shown in Fig.1. The core device was the MRI system (Varian, Inc Palo Alto, CA, USA), which was used for visualizing methane hydrate formation and dissociation process. And the MRI was operated at 400 MHz with a magnetic field strength of 9.4 Tesla, the standard spin echo pulse to obtain the two-dimensional proton density weighted image. MRI images were constructed by a spin echo multi-slice pulse sequence (SEMS) (Wang *et al.*, 2017), and the experimental parameters were: echo time (TE) 4.39 ms, repetition time (TR) 1000 ms, image data matrix (RO \times RE) 128 \times 128, field of view (FOV) 30 mm \times 30 mm with 2.0 mm thickness. The sequence acquisition time was 2.14 min for per vertical section image and 3.2 min for per cross section image. A high-pressure polyimide tube with a maximum pressure limitation of 13.0 MPa as the reactor had an effective height of 200 mm and diameter of 16 mm. And the reactor was surrounded by a heat preservation jacket in which the coolant circulates continually to keep the tube at required temperature.

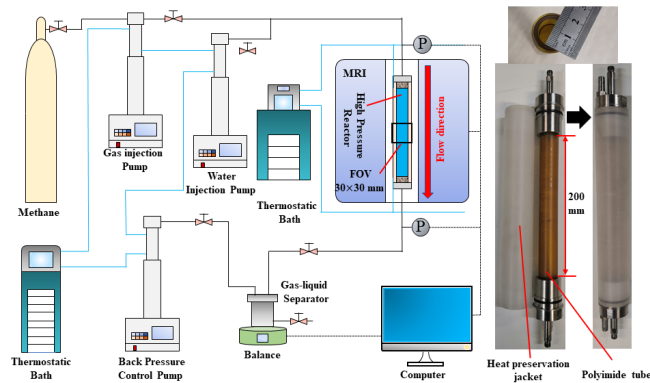


Fig. 1 . Schematic of the MRI apparatus.

Three high-precision syringe pumps (260D, Teledyne ISCO Inc, Lincoln, NE, USA) were used in the experiment to inject methane gas and deionized/seawater into the reactor and control the back-pressure of the reactor. Two thermostatic baths (FL300 and FL 25, JULABO, Seelbach, Germany) were used to control the temperature of high precision pump and the reactor. The pressure sensors (3510 CF, Emerson Electric Co., Ltd., St. Louis, USA) with an accuracy of $\pm 0.05\%$ were connected at the inlet and outlet of the reactor to measure the pressure. According to the results from the core analysis of SHSC-4 (Shenhu area of South China Sea), the mean effective porosity within interval “a” is 35% (Li *et al.*, 2018). Therefore, the glass beads (As-One Co., Ltd., Japan) with a porosity of 35.4% (BZ02) was used to simulate the porous media of marine environment, giving a diameter of 0.177~0.250 mm, so that the maximum of hydrate saturation in theory is higher than 35%. The seawater (deionized water with a salt mass fraction of 3.5%) was used during the flow process, which was more closed to the actual marine environment. In addition, the methane gas with a purity of 99% used in the experiments was produced by Dalian Special Gases Company.

2.2 Procedures

Hydrate sample was made through sand filling, vacuum pumping, water saturation, water displacement and pressurization. Firstly, the glass beads were compacted into the reactor, and the reactor was vacuumed for an hour. Secondly, the outlet valve of the reactor was closed, and the reactor inlet was connected with the water injection pump, the pressure and temperature were constant at 6.0 MPa, 274.15 K, respectively. This

was the water saturation process and maintained for about 30 min. Thirdly, closed the water injection pump and opened the reactor outlet value, the reactor pressure dropped to atmosphere. The water in the reactor was displaced to the initial water saturation around 39% using gas injection pump, the initial pressure of gas injection pump is 2.5 MPa. Finally, closed the reactor outlet value and maintained the pressure at 6.0 MPa using gas injection pump, the hydrate formation process began at this point. The entire process was recorded by MRI system and the hydrate saturation (S_h) could be calculated by mean intensity (MI) value through follow equation (*Chen et al. , 2021*):

$$S_h = 1.25 \times \frac{(I_0 - I_i)}{I_0} \times S_{w0} \times 100\% \quad (1)$$

$$S_{w0} = \frac{I_0}{I_{\text{full}}} \quad (2)$$

where I_0 , I_{full} and I_i were MI values of initial water saturation, complete water saturation and water saturation at time i , respectively. S_{w0} represented initial water saturation and can be calculated by equation (2). Additionally, the water saturation at time i (S_{wi}) can be calculated as follow:

$$S_{wi} = \frac{I_i}{I_{\text{full}}} \quad (3)$$

Table 1 . Conditions and resultes of hydrate sample in all cases.

Case	1	2	3	4	5	6	7
Hydrate saturation (%)	35.8	36.9	34.7	34.8	34.3	35.4	34.6
Water saturation (%)	49.2	50.8	52.8	49.8	57.3	54.9	55.8
Pressure (MPa)	6.0	6.0	6.0	6.0	6.0	6.0	6.0
Temperature (K)	274.15	274.15	274.15	274.15	274.15	274.15	274.15

The hydrate saturation in hydrate reservoir is usually very high, according to the geological exploration results (*Lpa et al. , 2019*). Thus, when the S_h reached about 35%, opened the outlet value of the reactor immediately, so the pressure in the reactor was controlled by the back pressure pump, this was the preparation for the gas–seawater flow. At 274.15 K, the phase equilibrium pressure of methane hydrate in seawater was 3.18 MPa (*Lafond et al. , 2012*), the back pressure in this study is 3.5 MPa or 4.0 MPa, which are all above the methane hydrate phase equilibrium pressure. The hydrate reservoir was usually in the state of water saturation (*Almenningen et al. , 2018; Chong et al. , 2017*). Therefore, to better simulate the academician state of hydrate in marine environment, the seawater was injected into the reactor using high–precision water injection pump at the flow rate of 0.5 ml/min. The seawater flow rate was low enough so that it can be considered that there was no hydrate decomposition during this process (*Chen et al. , 2019c*). After that, the gas and seawater were injected into the reactor at the same time using pumps. The temperature of injected methane gas and seawater was 273.95 K, which was slightly below the reservoir temperature, for the purpose to avoid the influence of heat injection on hydrate dissociation. The hydrate formation datas are shows in Table 1, it was obviously that all experimental conditions were inside the hydrate thermodynamic stable area to avoid the dissociation of hydrate due to other reasons (depressurization, temperature rise).

Results and discussion

Methane gas and seawater were injected into the hydrate–bearing sediments to simulate the gas and seawater

ascending in the seafloor sediments. Thus, gas–water two phase flow is a method to verify the sealing effect of hydrate reservoir. The water–saturated hydrate samples were made by injecting water into hydrate samples, as shown in Fig. 2. Furthermore, the gas–seawater flow rate ratio was constant at 4 for all Cases. The real–time characteristics of hydrate reservoir state was investigated using MRI visualization technology.

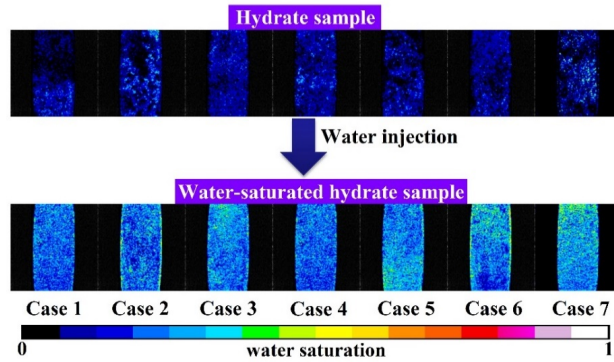


Fig. 2 . Initial hydrate reservoir conditions in all cases.

3.1 Methane–containing fluid flow characteristics inhydrate–bearing reservoirs

The free methane gas in the deep ocean floor is bound to migrate upward, and the gas migration also drives the movement of seawater in the sediments (*Su et al.* , 2012). We simulate gas–water migration by injecting gas and water into hydrate–bearing sediments, the experimental conditions of Cases 1–3 are shown in Table 2. The inlet pressure is increasing at the beginning, and large gas–water flow rate makes inlet pressure increase faster, as shown in Fig. 3, because the injection velocity of gas–water is larger than the seepage velocity of hydrate–bearing sediments. In Case 1, the methane gas and seawater were injected into the hydrate–bearing reservoir at the flow rate of 4–1 ml/min. After 52 min, the inlet pressure decreased, and the inlet pressure kept the same with outlet pressure at 136 min, fluids flow through the reservoir smoothly. The outlet flux curve of Case 1 increased and seawater flowed out of the reactor continually, indicating the hydrate reservoir had no sealing effect during gas–water flow process in Case.

Table 2. Experimental conditions and results of Cases 1–3.

Case	Fluid flow conditions	Maximum pressure increase	Hydrate change	Final flow
1	4 ml/min seawater & 1 ml/min methane	1.76 MPa	dissociation	flow thro
2	2 ml/min seawater & 0.5 ml/min methane	6.68 MPa	reformation and dissociation	hindranc
3	1 ml/min seawater & 0.25 ml/min methane	9.50 MPa	reformation	hindered

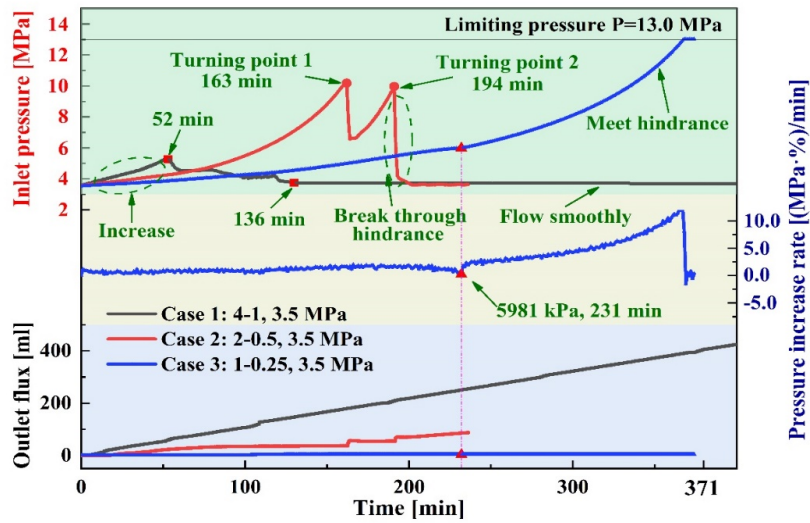


Fig. 3 . Characteristics of pressure at reactor inlet and reactor outlet flux

In Case 2, the inlet pressure reached about 10.0 MPa twice at the gas–water flow rate of 2–0.5 ml/min, and finally the inlet pressure dropped the same as outlet pressure. The inlet pressure increased before 163 min (turning point 1), and the seawater accumulated in the reservoir because the slope of outlet flux was decreased gradually. The inlet pressure increase indicating capillary sealing effect (*Liu* , 2007) appeared in the hydrate reservoir, and the reservoir permeability decreased which was caused by the hydrate saturation increase in the sediments (*Mahabadi et al.* , 2019). But the capillary sealing effect of hydrate reservoir was not stable, the hydrate hydrate saturation was not high enough, the hydrate–containing sealing layer was broken through at 163 and 194 min, respectively, and caused inlet pressure decrease, the whole process is shown in Fig. 4. The break through (BT) pressure were 6.68 MPa, 6.46 MPa, respectively, and the reason of this phenomenon are the large pressure difference on both sides of hydrate reservoir (*Liu* , 2007) and the incompletely formation of hydrate–containing sealing layer.

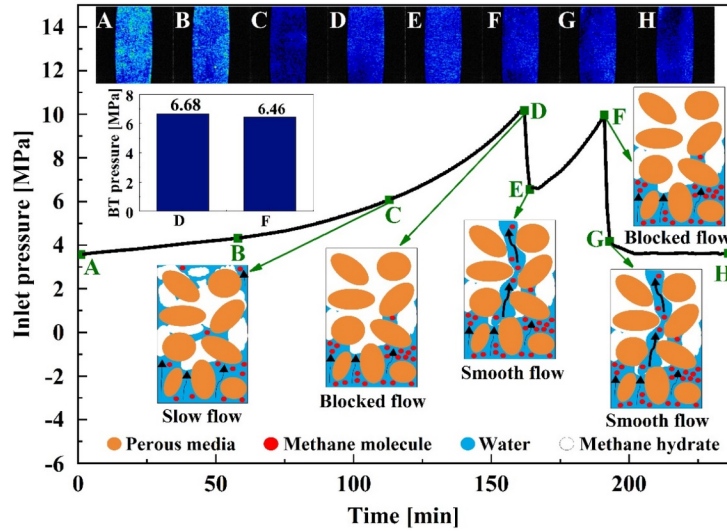


Fig. 4 . Breakthrough of hydrate-containing sealing layer in Case 2

In Case 3, the gas-water flow rate was 1–0.25 ml/min. It could be found the inlet pressure kept increasing, so as the pressure difference between reactor inlet and outlet. It was obvious there was a fluctuation in pressure increase rate curve (231 min, and the inlet pressure was 5.98 MPa), and the curve tended to be stable before 231 min, but it got larger after 231 min. After 231 min, the seawater can't flow through the reactor, the hydrate reservoir possessed sealing effect to fluids after 231 min. The pressure increase rate at i min can be calculated by Eq. (4):

$$R_i = \frac{P_i - P_{i+t}}{t} \bullet \% \quad (4)$$

The inlet pressure increased to 13.0 MPa at last, due to the limitation of experimental, thus, at least 9.0 MPa pressure difference existed on both sides of the hydrate reservoir. It's important to emphasize this pressure difference was not caused by gravity, and the sealing effect of hydrate-bearing reservoir, which is shown as pressure difference, represents the ability of hydrate reservoir to trap underlying gas. In addition, this pressure difference providing the development condition of higher-pressure gas reservoir under hydrate layer, and the pressure difference between hydrate zone and gas zone must be considered during hydrate exploitation process.

The reservoir condition could be visually observed by MRI, because the MRI can only acquire images of the ^1H contained in liquid water (*Wang et al.*, 2020), and the hydrate saturation could be calculated using Eq. (1). Fig. 5(a) shows the characteristics of water distributions in FOV, and Fig. 5(b) reflects the real-time characteristics of hydrate saturation. When the gas-water flow rate was 4–1 ml/min (Case 1), the MRI images brightened gradually after 52 min, and the hydrate saturation decreased, indicating the hydrate dissociated during the gas-water flow process. The reservoir condition (274.15 K, 3.5 MPa) was in hydrate thermodynamic stable area, thus, the driving force for hydrate dissociation was the chemical potential difference between seawater phase and hydrate phase (*Chen et al.*, 2019a; *Chen et al.*, 2019b). The chemical potential difference is caused by the inadequate dissolution of methane gas (*Sun et al.*, 2020b; *Zheng*, 2007). Hydrate dissociation is the reason that the inlet pressure decreased after 52 min. Thus, hydrate dissociation will reduce or even disappear the sealing effect of hydrate-bearing sediments. For Case 2, the MRI images had no noticeable darkening area, and hydrate saturation curve fluctuated, indicating small amount of hydrate forms. In the gas-water flow rate of 2–0.5 ml/min, hydrates were not always formed or decomposed, it was in an approximate equilibrium state. Thus, the hydrate-containing

sealing layer was broken through under large pressure difference. For Case 3, it can be seen that the MRI images going to darken gradually over time, and the hydrate saturation curve presented an increasing trend. Hydrate formed during the gas–water flow process at the flow rate of 1–0.25 ml/min. The inlet pressure was also increased to 13.0 MPa, it could be concluded that hydrate formation enhanced the sealing effect of hydrate–bearing sediments. Hydrate formed continuously even though the sealing effect had been existed in hydrate reservoir. Furthermore, the continuously increasing inlet pressure provided larger driving force for hydrate formation. The hydrate formation before the turning point formed the hydrate–containing sealing layer; the hydrate formation before the turning point further enhanced the hydrate–containing sealing layer. After the turning point (231 min), the seawater can’t flow through the reactor, indicating the reservoir had sealing effect. The mechanism of sealing effect is because that the sediment pores were occupied by more hydrate and became smaller, the residual water in the sediment created capillary forces in the narrow pore space, which blocked the gas–water migration.

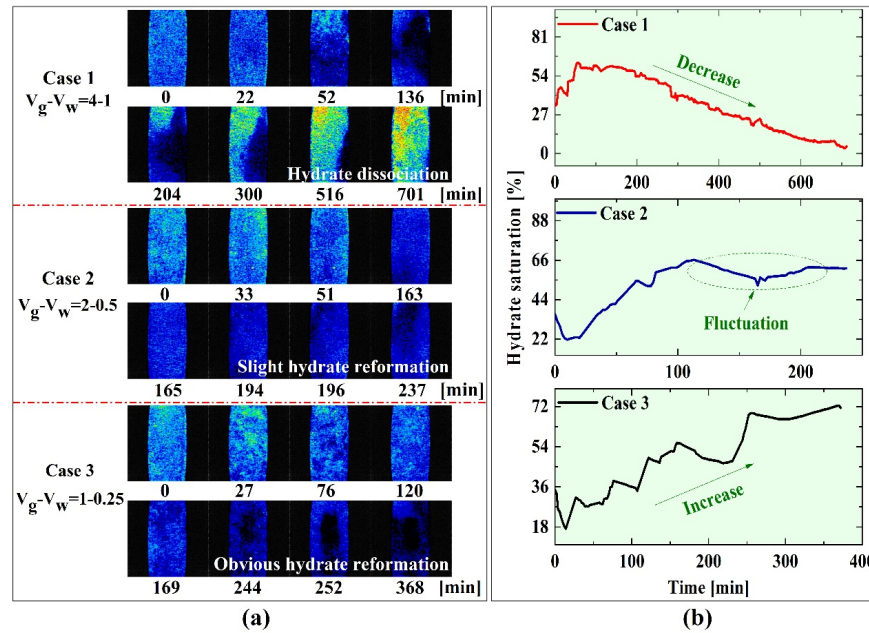


Fig. 5 . Micro-images during the gas–seawater flow process in Cases 1–3: (a) MRI images; (b) hydrate saturation

In conclusion, the hydrate–containing sealing layer formed when the gas–water flow rate is 1–0.25 ml/min. The seawater is full contact with the methane gas in lower gas–water flow rate, methane saturation in seawater is high enough to induce the hydrate reformation. The decrease of pore volume leads to the increase of capillary force, thus, sealing layer formal formed, this is the formation mechanism of hydrate–containing sealing layer. Then, the hydrate continued to form in the reservoir which enhanced the sealing layer and makes it more difficult to be destroyed.

3.2 Sealing characteristics of hydrate–bearing reservoir on external fluids

Hydrate reformation is the reason that sealing effect exists in hydrate–bearing sediments. We increased the hydrate formation rate by increasing reservoir pressure to 4.0 MPa, the characteristics of hydrate–containing sealing layer was investigated, the experimental conditions of Cases 4 and 5 are shown in Table 3. Take the injection volume as the reference value, it was found that high flow rate (Case 5) has hysteresis phenomenon compared with low flow rate (Case 4), but higher flow rate consumed less time.

Table 3. Experimental conditions and results of Cases 4 and 5.

Case	Fluid flow conditions	Maximum pressure increase	Hydrate change	Final flow state
4	2 ml/min seawater & 0.5 ml/min methane	9.00 MPa	reformation	hindered at 94 min
5	4 ml/min seawater & 1 ml/min methane	9.00 MPa	reformation	hindered at 54 min

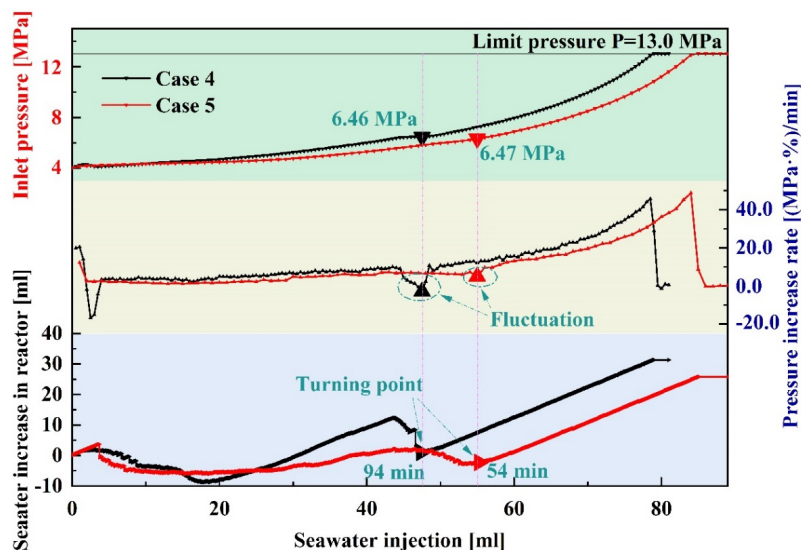


Fig. 6 . Characteristics of pressure at reactor inlet and seawater increase in reactor

As shown in Fig. 6, the turning points appeared at 94 and 54 min in Cases 4 and 5, respectively. After the turning point, the seawater won't flow out of the reservoir outlet, the hydrate reservoir had sealing effect. The gas-water flow rates of Cases 4 and 5 were the same as Cases 2 and 1, respectively. However, hydrate-containing sealing layer formed only in Cases 4 and 5, because higher reservoir pressure provide larger driving force for hydrate formation (*Ma et al.*, 2020). It also indicated that higher pressure will promote the formation of hydrate-containing sealing layer than low gas-water flow rate. Because the higher pressure can enhance the mass transfer between the gas and seawater, and enhance hydrate formation during gas-water flow process. Moreover, the pressure increases rate curve had a fluctuation at the turning point, and increase rate of inlet pressure was decreased, this fluctuation also appeared in Case 3. Furthermore, there is a certain regularity in the pressure difference between the reactor inlet and outlet at the time of hydrate-containing sealing layer is formal formed, as shown in Fig. 7. The mean value of pressure different is 2.47 MPa. In this study, the pressure difference at turning point is independent of reservoir pressure, it can be used as a marker to judge the formation of hydrate seal layer during the experiment.

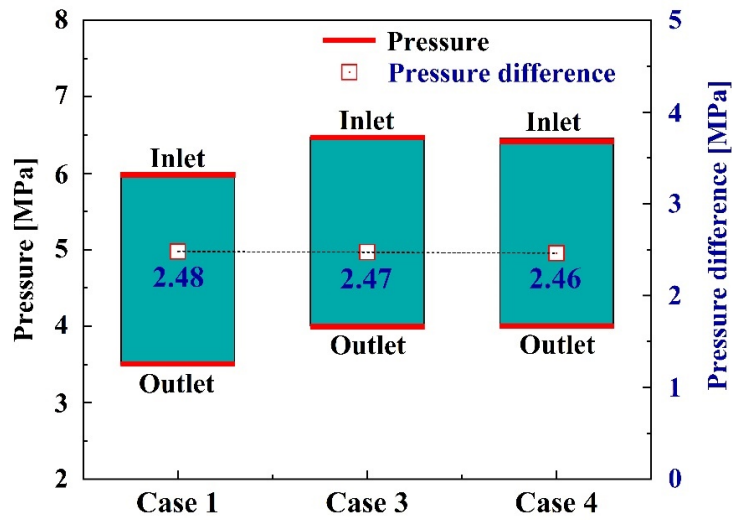


Fig. 7 . Pressure difference values at onset time of sealing layer formation

Fig. 8 shows the variation characteristics of hydrate saturation in FOV during the gas–water injection process of cases 4 and 5. The MRI images is getting darker in Case 5 and hydrate saturation present an increasing trend, thus, hydrate formed during the gas–water flow process and hydrate–bearing reservoir had sealing effect. However, hydrate saturation didn’t show an obviously increasing trend in Case 4, though the sealing effect existed after 94 min. It could be found that there was a significant change in the lower left corner of FOV in Case 4, so we analyzed the change in MI value of Line 1. The small distance of MI value ($0\sim 4.2$ mm) is obviously reduced, indicating that hydrate formed in this area and consumed the pore water. The reason for sealing effect exists in Case 4 was also caused by hydrate formation, but hydrate formation was not concentrated in the FOV, and thought it was below the FOV. To further analyze the reservoir state, multi–level MRI image (4 layers) was carried out by adjusting the position of the reactor.

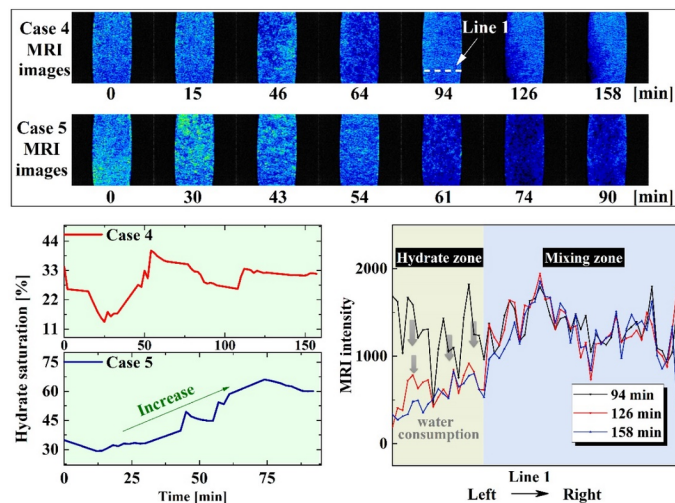


Fig. 8 . Main results of Cases 4 and 5

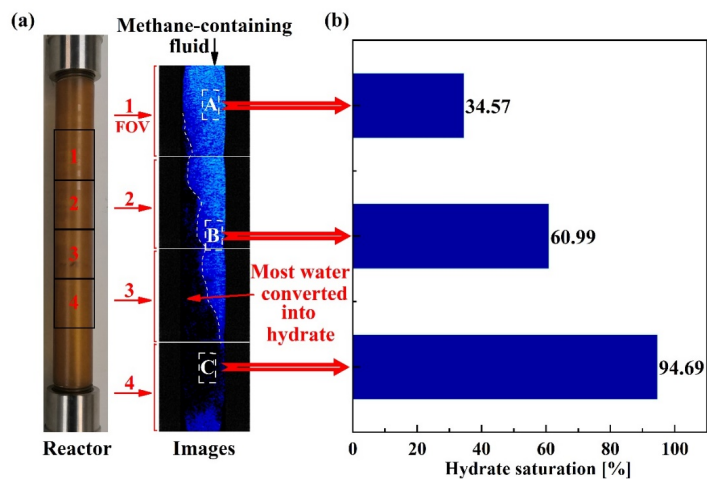


Fig. 9 . (a) multi-level MRI images in Case 4; (b) hydrate saturation in different areas

Fig. 9(a) was the multi-level MRI images of reactor after 158 min in Case 4. The camera on the MRI device remained stationary, and moved the reactor 30 mm upwards after each shot, for the reason the FOV was 30 mm× 30 mm, complete reservoir status is presented by this operation. The gas-water injection was

stopped and the inlet pressure was constant at 13.0 MPa during the whole shooting process. Significant brightness differences could be found in the hydrate reservoir. By comparing the hydrate saturation in different areas, as shown in Fig. 9(b), the hydrate saturation was higher in farther area along the gas–water injection direction. The pore seawater in area C was almost consumed up, tiny amount of seawater still remained in the hydrate reservoir and it is too saline to form hydrate, it was hydrate zone. The brighter area (areas A and B) compared with area C was water zone (seawater, hydrate, gas coexisted). The free gas was hindered out of the reactor inlet. Thus, the hydrate reservoir can be divided into three layers. This is very similar to the hydrate reservoir with three structures in the South China Sea: gas hydrate layer; mixing layer consisting of hydrates, free gas and seawater; free gas layer coexists from top to bottom (*Qin et al.*, 2020). And the experimental phenomenon is consistent with the model for free gas migration presented by Liu et al (*Liu and Flemings*, 2006).

3.3 Effects of hydrate saturation change on the sealing layer formation process

In Cases 3, 4, 5, the inlet pressure increased as soon as the gas–water flowed, indicating the hydrate–containing sealing layer formed at the beginning. Thus, we investigated the effects of hydrate saturation change on sealing layer by increasing seawater injection rate ratio, the experimental conditions of Cases 6 and 7 are shown in Table 4. When seawater flow in hydrate reservoir was enhanced, the reservoir won't produce sealing effect during flow process. The gas–water process was divided into two stages (see Fig. 10): in the first stages the gas–water flow rate was 1–2 ml/min, in the second stage, the gas–water flow rate was 2–0.5 ml/min in Case 5 and 4–1 ml/min in Case 6, respectively.

Table 4. Experimental conditions and results of Cases 6 and 7.

Case	Fluid flow conditions in step 1	Fluid flow conditions in step 2	Hydrate change
6	1 ml/min seawater & 2 ml/min methane	2 ml/min seawater & 0.5 ml/min methane	dissociation in step 1 and re
7	1 ml/min seawater & 2 ml/min methane	4 ml/min seawater & 1 ml/min methane	dissociation in step 1 and re

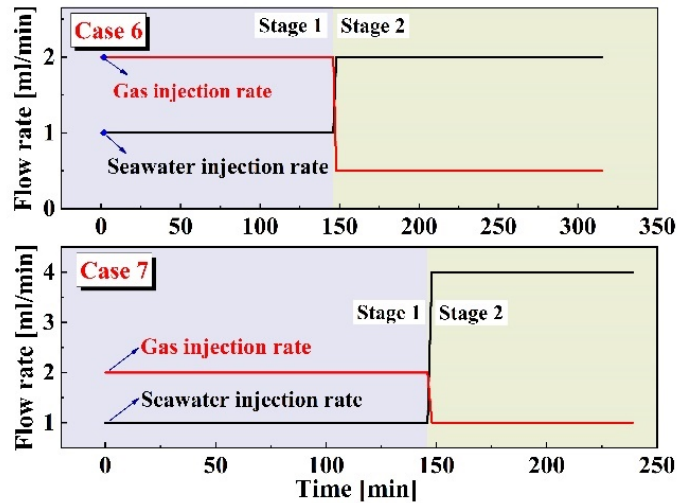


Fig. 10 . Gas–water injection rates in Case 6 and Case 7

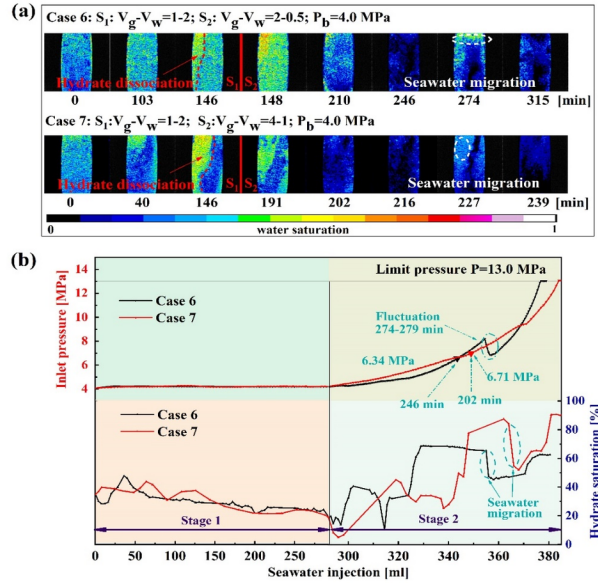


Fig. 11 . MRI images and inlet pressure and hydrate saturation changes in Cases 6 and 7

Fig. 11 shows MRI images in FOV and the characteristics of hydrate saturation during the whole flow process. In the stage 1 (S_1), the inlet pressure of both cases remained stable around 4.0 MPa. However, the inlet pressure is slightly higher than the back pressure (about 4.2 MPa), because the contact of seawater and hydrate causes the capillary force in the sediments. The MRI images of S_1 brightened, indicating the hydrate dissociated during the gas–water flow process with the flow rate of 1–2 ml/min. Because the large amounts of seawater flow enhanced the mass transfer between hydrate phase and seawater phase, the driving force is the chemical potential difference caused by low methane concentration in seawater (*Sun et al.* , 2020a; *Yang et al.* , 2019). Meanwhile, the random distribution of hydrate in porous media was the reason that the seawater–hydrate interface in Case 6 and Case 7 was different (*Zhang et al.* , 2019). The hydrate dissociation areas in Fig. 11(a) could be considered the chimney in the hydrate reservoir (*Torres et al.* , 2004), the reservoir had no sealing effect and showed well permeability characteristics.

In the stage 2, the gas–water flow in hydrate–bearing sediments with chimney due to hydrate dissociation in stage 1, it was obvious that the reactor inlet pressure was increasing, shown in Fig. 11(b), and the corresponding MRI images went dimmed, hydrate saturation increased. As the seawater flow rate decreased and methane gas flow rate increased, the methane dissolved more fully in seawater. Thus, the hydrate formed inside the hydrate thermodynamically stable area, the gas–water flow process in S_2 was the formation process of hydrate–containing sealing layer. In Case 6, no more seawater flowed out of the reactor after 246 min, hydrate–containing sealing layer had sealing effect at this moment. The inlet pressure fluctuated in 274–279 min, and seawater flowed into the FOV. Under the driving of pressure difference, the hydrate–containing sealing layer was partially destroyed and seawater migrated in the reservoir, but the seawater did not break through the sealing layer. The hydrate continuously formed after 279 min, the pore volume is reduced, thus the inlet pressure increased faster. In Case 6, the turning point appeared at 202 min, the pressure difference of in and out is 2.34 MPa in Case 5 and 2.71 MPa in Case 6, respectively. They were all close to the mean value of pressure different (2.47 MPa), the pressure difference of in and out could be a marker to judge the formation of hydrate–containing sealing layer. In hydrate–bearing sediments, the hydrate–containing sealing layer can be formed when hydrate reforms in hydrate reservoir, even though hydrate has dissociated before.

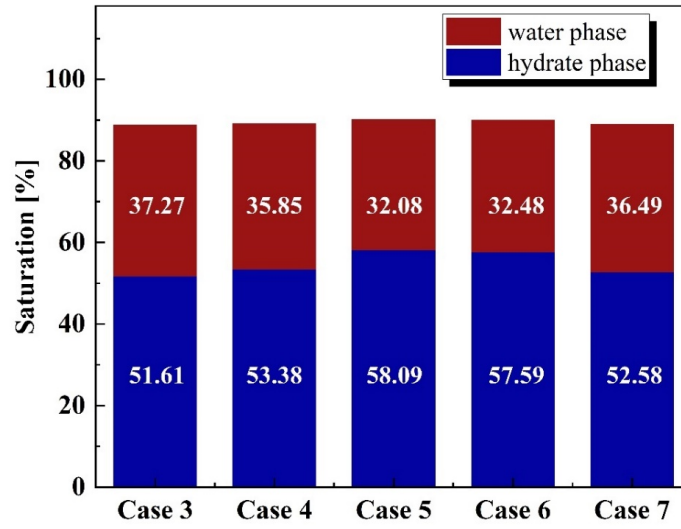


Fig. 12 . Saturations of hydrate and water phases below hydrate zone at sealing onset in different cases.

The hydrate-containing sealing layer formed in cases 3, 4, 5, 6, 7 for the reason that hydrate reformed in hydrate-bearing sediments. Hydrate saturation is the most direct criterion to judge whether hydrate reservoir has sealing effect. Seawater is almost consumed up of Area A in Fig. 9(a) and hydrate saturation is close to 100%, thus, we choose Area B in Fig. 9(a) as reference. Hydrate saturation at the turning point for cases 3, 4, 5, 6, 7 are shown in Fig. 12. It is obvious that hydrate saturation is above 51.61%, we consider this is the lowest hydrate saturation that reservoir has sealing effect, and the water saturation is between 32.08% and 37.27%. If the hydrate saturation is higher than 37.27%, sealing effect of hydrate-containing sealing layer may not exist due to insufficient conversion of water to hydrate, and the water saturation will decrease as the hydrate continues to form in hydrate-containing sealing layer.

Conclusion

In this study, the existence of hydrate-containing sealing layer is firstly experimentally confirmed using MRI visualization device by injecting methane gas and seawater into hydrate reservoirs at 3.5 and 4.0 MPa and 274.15 K. The reformation of hydrates at low gas-water flow rate or high reservoir pressure environment (hydrate saturation is higher than 51.61%) is confirmed contributed to the occurrence of sealing effect that hinders the external fluids flowing through the reservoir. Near all of pore water has been consumed to form hydrates in the sealing layer. In addition, the same pressure difference of approximately 2.47 MPa between reactor inlet and outlet was found in the different experimental cases that process sealing layers and could be a significant marker suitable for hydrate reformation. This is also a novel method, put forward in this study, to form hydrate-containing sealing layer in experimental condition. When the hydrates dissociate by high-rate gas-water flow, the sealing effect does not exist any longer. The entire natural gas hydrate reservoir, which includes three-layer distribution of hydrate, water, and gas from top to bottom, recognized by BSR is perfectly demonstrated by MRI images in this study, and A pressure difference of at least 9.0 MPa is found existing on both sides of the sealing layer, providing the development condition of higher-pressure gas reservoir under hydrate layer. The results of this study reveal the key reason why free gas can exist stably underling hydrate layer in nature and can guide the safe joint exploitation of hydrate and gas reservoirs.

Acknowledgments

This project was financially supported by the National Natural Science Foundation of China (51822603, U19B2005), Liao Ning Revitalization Talents Program (XLYC1907096), the Innovation Foundation of Science and Technology of Dalian (2019J11CY012) and the Fundamental Research Funds for the Central Universities of China (DUT21ZD103).

Declaration of Competing Interest

The authors declare that they have no known competing financial interests or personal relationships that could have appeared to influence the work reported in this paper.

CRedit authorship contribution statement

Guojun Zhao : Methodology, Visualization, Writing original draft, Writing review & editing. **Huiru Sun** : Data curation. **Mingjun Yang** : Formal analysis, Supervision. **Jia-nan Zheng** : Conceptualization, Investigation. **Xin Lv** : Resources. **Yongchen Song** : Supervision.

References

- Almenningen, S., J. Gauteplass, P. Fotland, G. L. Aastveit, T. Barth, and G. Ersland (2018), Visualization of hydrate formation during CO₂ storage in water-saturated sandstone(J), *International Journal of Greenhouse Gas Control* , 119 , 678-687. <https://doi.org/10.1016/j.ijggc.2018.11.008>
- Buleiko, V. M., B. A. Grigoriev, and V. A. Istomin (2017), Capillary effects on phase behavior of liquid and gaseous propane and dynamics of hydrate formation and dissociation in porous media, *Fluid Phase Equilib.* , 441 , 64-71, doi:10.1016/j.fluid.2017.01.026. <https://doi.org/10.1016/j.fluid.2017.01.026>
- Chen, Z. Liu, H. Sun, G. Zhao, and M. Yang (2021), The synthetic effect of traditional-thermodynamic-factors (temperature, salinity, pressure) and fluid flow on natural gas hydrate recovery behaviors(J), *Energy* (1), 121147. <https://doi.org/10.1016/j.energy.2021.121147>
- Chen, H. Sun, K. Li, D. Wang, and M. Yang (2019a), Experimental investigation of natural gas hydrate production characteristics via novel combination modes of depressurization with water flow erosion(J), *Fuel* , 252 , 295-303. <https://doi.org/10.1016/j.fuel.2019.04.120>
- Chen, H. Sun, H. Zhou, M. Yang, and D. Wang (2019b), Effects of pressure and sea water flow on natural gas hydrate production characteristics in marine sediment(J), *Applied Energy* , 238 (MAR.15), 274-283. <https://doi.org/10.1016/j.apenergy.2019.01.095>
- Chen, M. Yang, H. Sun, P. Wang, and D. Wang (2019c), Visualization study on the promotion of natural gas hydrate production by water flow erosion(J), *Fuel* , 235 (JAN.1), 63-71. <https://doi.org/10.1016/j.egypro.2019.01.586>
- Chong, Z. R., Z. Yin, J. Tan, and P. Linga (2017), Experimental investigations on energy recovery from water-saturated hydrate bearing sediments via depressurization approach(J), *Applied Energy* , 204 , 1513-1525. <https://doi.org/10.1016/j.apenergy.2017.04.031>
- Clennell, M. B., P. Henry, M. Hovland, J. S. Booth, and M. Thomas (1999), Formation of natural gas hydrates in marine sediments: 1. Conceptual model of gas hydrate growth conditioned by host sediment properties(J), *Annals of the New York Academy of Sciences* , 104 (1), 22985-23003. <https://doi.org/10.1029/1999JB900175>
- Collett, T. S., and G. D. Ginsburg (1998), Gas Hydrates In the Messoyakha Gas Field of the West Siberian Basin - A Re-Examination of the Geologic Evidence(J), *International Journal of Offshore & Polar Engineering* , 8 (1), 22-29. Paper Number: ISOPE-98-08-1-022
- Dillon, W. P., J. A. Grow, and C. K. Paull (1980), Unconventional gas hydrate seals may trap gas off southeast U.S(J), *Oil and Gas Journal* , 78 (1), 124-130. [https://doi.org/10.1016/S0025-3227\(99\)00128-0](https://doi.org/10.1016/S0025-3227(99)00128-0)
- Flemings, P. B., X. Liu, and W. J. Winters (2003), Critical pressure and multiphase flow in Blake Ridge gas hydrates(J), *Geology* , 31 (12), 1057-1060. <https://doi.org/10.1130/G19863.1>

- Graver, T., G. Moridis, and S. A. Holditch (2008), Analysis of Reservoir Performance of Messoyakha Gas Hydrate Field(D), Proceedings of the International Offshore and Polar Engineering Conference.
- He, T., G. D. Spence, W. T. Wood, M. Riedel, and R. D. Hyndman (2009), Imaging a hydrate-related cold vent offshore Vancouver Island from deep-towed multichannel seismic data(J), *Geophysics* ,74 (2), B23. <https://doi.org/>
- Heeschen, K. U., R. W. Collier, M. Angelis, E. Suess, G. Rehder, P. Linke, and G. P. Klinkhammer (2005), Methane sources, distributions, and fluxes from cold vent sites at Hydrate Ridge, Cascadia Margin(J), *Global Biogeochemical Cycles* , 19 . <https://doi.org/10.1029/2004GB002266>
- Helgerud, M. B., W. F. Waite, S. H. Kirby, and A. Nur (2011), Measured temperature and pressure dependence of V-p and V-s in compacted, polycrystalline sI methane and sII methane-ethane hydrate(J), *Canadian Journal of Physics* , 81 (1-2), 47-53. <https://doi.org/10.1139/P03-016>
- Hornbach, M. J., D. M. Saffer, and W. S. Holbrook (2004), Critically pressured free-gas reservoirs below gas-hydrate provinces(J), *Nature* , 427 (6970), 142-144. <https://doi.org/10.1038/nature02172>
- Huang, B. X., W. C. Xue, Y. Z. Wang, and T. Zhang (2011), Review of Theory and Practice on Natural Gas Hydrate(J), *Advanced Materials Research* , 361-363 , 149-160. <https://doi.org/10.4028/AMR.361-363.149>
- Lafond, P. G., K. A. Olcott, E. D. Sloan, C. A. Koh, and A. K. Sum (2012), Measurements of methane hydrate equilibrium in systems inhibited with NaCl and methanol(J), *Journal of Chemical Thermodynamics* ,48 , 1-6. <https://doi.org/10.1016/j.jct.2011.12.023>
- Li, J., et al. (2018), The first offshore natural gas hydrate production test in South China Sea(J), *China Geology* , 1 (1), 5-16, doi:10.31035/cg2018003. <https://doi.org/10.31035/cg2018003>
- Liang, J. Q., W. Deng, J. A. Lu, Z. G. Kuang, and M. M. Meng (2020), A fast identification method based on the typical geophysical differences between submarine shallow carbonates and hydrate bearing sediments in the northern South China Sea(J), *China Geology* , 3 (1), 16-27. <https://doi.org/10.31035/cg2020021>
- Liu (2007), Dynamic multiphase flow model of hydrate formation in marine sediments(J), *Journal of Geophysical Research Solid Earth* ,112 (B3), B03101. <https://doi.org/10.1029/2005JB004227>
- Liu, and P. B. Flemings (2006), Passing gas through the hydrate stability zone at southern Hydrate Ridge, offshore Oregon(J),*Earth & Planetary Science Letters* , 241 (1-2), 211-226. <https://doi.org/10.1016/j.epsl.2005.10.026>
- Liu, Liping, SUN, Zhilei, ZHANG, Lei, WU, Nengyou, Yichao, and Qin (2019), Progress in Global Gas Hydrate Development and Production as a New Energy Resource(J), *Acta Geologica Sinica(English Edition)* ,v.93 (03), 231-255. <https://doi.org/10.1111/1755-6724.13876>
- Logan, G. A., A. T. Jones, J. M. Kennard, G. J. Ryan, and N. Rollet (2010), Australian offshore natural hydrocarbon seepage studies, a review and re-evaluation(J), *Marine & Petroleum Geology* ,27 (1), 26-45. <https://doi.org/10.1016/j.marpetgeo.2009.07.002>
- Lpa, B., B. Ksa, and A. Akj (2019), Estimate of gas hydrate saturations in the Krishna-Godavari basin, eastern continental margin of India, results of expedition NGHP-02(J), *Marine and Petroleum Geology* ,108 , 581-594. <https://doi.org/10.1016/j.marpetgeo.2018.12.009>
- Ma, S., J. N. Zheng, M. Tian, D. Tang, and M. Yang (2020), NMR quantitative investigation on methane hydrate formation characteristics under different driving forces(J), *Fuel* , 261 (Feb.1), 116361-116364. <https://doi.org/10.1016/j.fuel.2019.116364>
- Mahabadi, N., S. Dai, Y. Seol, and J. Jang (2019), Impact of hydrate saturation on water permeability in hydrate-bearing sediments(J),*Journal of Petroleum Science and Engineering* , 174 , 696-703. <https://doi.org/10.1016/j.petrol.2018.11.084>

- Makogon (2010), Natural gas hydrates – A promising source of energy(J), *Journal of Natural Gas Science and Engineering* , 2 (1), 49-59. <https://doi.org/10.1016/j.jngse.2009.12.004>
- Makogon, S. A. Holditch, and T. Y. Makogon (2005), Russian field illustrates gas-hydrate production(J), *Oil and Gas Journal* ,103 (5), 43-47. <https://doi.org/WOS:000226889700015>
- Merey, ü., and S. N. Longinos (2018), Numerical simulations of gas production from Class 1 hydrate and Class 3 hydrate in the Nile Delta of the Mediterranean Sea(J), *Journal of Natural Gas Science and Engineering* , 52 , 248-266. <https://doi.org/10.1016/j.jngse.2018.01.001>
- Milkov, A. V., G. R. Dickens, G. E. Claypool, Y. J. Lee, W. S. Borowski, M. E. Torres, W. Xu, H. Tomaru, A. Tréhu, and P. Schultheiss (2004), Co-existence of gas hydrate, free gas, and brine within the regional gas hydrate stability zone at Hydrate Ridge (Oregon margin): evidence from prolonged degassing of a pressurized core(J), *Earth & Planetary Science Letters* , 222 (3-4), 829-843. <https://doi.org/10.1016/j.epsl.2004.03.028>
- Ming, S., S. Zhibin, Z. Cuimei, W. Hongbin, W. Nengyou, Y. Rui, L. Jinqiang, Q. Shaohua, C. Xiaorong, and L. Jie (2017), Types, characteristics and significances of migrating pathways of gas-bearing fluids in the Shenhu area, northern continental slope of the South China Sea, *Acta Geol. Sin.-Engl. Ed.* , 91 (1), 219-231. <https://doi.org/10.1111/1755-6724.13073>
- Miyakawa, A., S. Saito, Y. Yamada, H. Tomaru, M. Kinoshita, and T. Tsuji (2014), Gas hydrate saturation at Site C0002, IODP Expeditions 314 and 315, in the Kumano Basin, Nankai trough(J), *Island Arc* ,23 (2), 142-156. <https://doi.org/10.1111/iar.12064>
- Moridis, G. J., M. B. Kowalsky, and K. Pruess (2007), Depressurization-Induced Gas Production From Class-1 Hydrate Deposits(J), *Society of Petroleum Engineers Reservoir Evaluation Andengineering* , 10 (05), 458-481. <https://doi.org/10.2118/97266-PA>
- Ning, F., N. Wu, S. Li, K. Zhang, Y. Yu, L. Liu, J. Sun, G. Jiang, C. Sun, and G. Chen (2013), Estimation of in-situ mechanical properties of gas hydrate-bearing sediments from well logging(J), *Petroleum Exploration & Development* , 40 (4), 542-547. [https://doi.org/ https://doi.org/10.1016/S1876-3804\(13\)60071-3](https://doi.org/https://doi.org/10.1016/S1876-3804(13)60071-3)
- Petersen, C. J., C. Papenberg, and D. Klaeschen (2007), Local seismic quantification of gas hydrates and BSR characterization from multi-frequency OBS data at northern Hydrate Ridge(J), *Earth and Planetary Science Letters* , 255 (3), 414-431. <https://doi.org/10.1016/j.epsl.2007.01.002>
- Pibo, S. U., J. Liang, Z. Zhang, and Z. Sha (2017), Analysis on the bright spots and dim out of seismic section for diffusion-type hydrate in Shenhu area(J), *Earth Science Frontiers* , 04 , 57-62. <https://doi.org/CSCD:6018712>
- Qiang, C., G. W. Hu, N. Y. Wu, C. L. Liu, Q. G. Meng, C. F. Li, J. Y. Sun, and Y. L. Li (2020), Evaluation of clayed silt properties on the behavior of hydrate production in South China Sea(J), *China Geology* , 3 (3), 362-368. <https://doi.org/10.31035/cg2020050>
- Qin, X. W., J. A. Lu, H. L. Lu, H. J. Qiu, J. Q. Liang, D. J. Kang, L. S. Zhan, H. F. Lu, and Z. G. Kuang (2020), Coexistence of natural gas hydrate, free gas and water in the gas hydrate system in the Shenhu Area, South China Sea(J), *China Geology* , 3 (2), 210-220. <https://doi.org/10.31035/cg2020038>
- Shi, Y., Q. Liang, J. Yang, Q. Yuan, X. Wu, and L. Kong (2019), Stability analysis of submarine slopes in the area of the test production of gas hydrate in the South China Sea(J), *China Geology* , 2 (3), 274-284, doi:10.31035/cg2018122. <https://doi.org/10.31035/cg2018122>
- Song, Y., P. Wang, L. Jiang, Y. Zhao, and M. Yang (2015), Methane hydrate formation/reformation in three experimental modes: A preliminary investigation of blockage prevention during exploitation(J), *Journal of Natural Gas Science & Engineering* , 27 , 1814-1820. <https://doi.org/10.1016/j.jngse.2015.11.009>
- Su, Z., Y. Cao, N. Wu, D. Chen, S. Yang, and H. Wang (2012), Numerical investigation on methane hydrate accumulation in Shenhu Area, northern continental slope of South China Sea(J), *Marine & Petroleum*

Geology , 38 (1), 158-165. <https://doi.org/10.1016/j.marpetgeo.2012.06.005>

Su, Z., Y. C. Cao, N. Y. Wu, L. M. Cathles, and D. F. Chen (2009), Numerical computation and case analysis of the venting process of free gas beneath hydrate layer(J), *Chinese Journal of Geophysics* ,52 (12), 3124-3131. <https://doi.org/10.3969/j.issn.0001-5733.2009.12.022>

Sun, H., B. Chen, and M. Yang (2020a), Effect of multiphase flow on natural gas hydrate production in marine sediment(J), *Journal of Natural Gas Science and Engineering* , 73 , doi:10.1016/j.jngse.2019.103066. <https://doi.org/10.1016/j.jngse.2019.103066>

Sun, H., B. Chen, G. Zhao, Y. Zhao, and M. Yang (2020b), Utilization of water-gas flow on natural gas hydrate recovery with different depressurization modes(J), *Fuel* , doi:10.1016/j.fuel.2020.119583. <https://doi.org/10.1016/j.fuel.2020.119583>

Tian, D., and X. Liu (2020), A new approach for the identification of gas hydrate in marine sediments(J), *Marine Geophysical Research* ,41 (3), 1-12. <https://doi.org/10.1007/s11001-020-09412-y>

Torres, M. E., K. Wallmann, A. Trehu, G. Bohrmann, W. S. Borowski, and H. Tomaru (2004), Gas hydrate growth, methane transport, and chloride enrichment at the southern summit of Hydrate Ridge, Cascadia margin off Oregon(J), *Earth and Planetary Science Letters* , 226 (1-2), 225-241. <https://doi.org/10.1016/j.epsl.2005.05.044>

Touil, A., D. Broseta, and A. Desmedt (2019), Gas hydrate crystallization in thin glass capillaries: Roles of supercooling and wettability, *Langmuir* , 35 (38), 12569-12581. <https://doi.org/10.1021/acs.langmuir.9b01146>

Wang, Y. Liu, Y. Zhao, Y. Zhang, and Y. Song (2020), Enhanced Mass Transfer by Density-Driven Convection during CO₂ Geological Storage,*Industrial & Engineering Chemistry Research* , 59 (19), 9300-9309. <https://doi.org/10.1021/acs.iecr.0c00525>

Wang, S. Wang, Y. Song, and M. Yang (2017), Methane Hydrate Formation and Decomposition Properties During Gas Migration in Porous Medium(J),*Energy Procedia* , 105 , 4668-4673. <https://doi.org/10.1016/j.egypro.2017.03.1012>

Xu, W., and C. Ruppel (1999), Predicting the occurrence, distribution, and evolution of methane gas hydrate in porous marine sediments(J),*Journal of Geophysical Research Solid Earth* , 104 (B3), 5081-5096. <https://doi.org/10.1029/1998JB900092>

Yang, H. Sun, B. Chen, and Y. Song (2019), Effects of water-gas two-phase flow on methane hydrate dissociation in porous media(J),*Fuel* , 255 , doi:10.1016/j.fuel.2019.115637. <https://doi.org/10.1016/j.fuel.2019.115637>

Yang, J. Wang, and Y. Jiang (2020), Experimental Study and Numerical Simulation of Overlying Layer Soil Failure Caused by Hydrate Decomposition(J), *ACS Omega* , 5 (48), 31244-31253. <https://doi.org/10.1021/acsomega.0c04619>

Zhang, L., L. Sun, M. Sun, X. Lv, and J. Zhao (2019), Analyzing spatially and temporally visualized formation behavior of methane hydrate in unconsolidated porous media(J), *Magnetic Resonance Imaging* , 61 , 224-230. <https://doi.org/10.1016/j.mri.2019.06.005>

Zhang., and D. R. McConnell (2010), Seismic Modeling Analysis and Characterization of a Gas Hydrate and Free Gas Mixed System in Green Canyon, Gulf of Mexico(J), *Proceedings of the Annual Offshore Technology Conference* , 2 , 1530-1541. <https://doi.org/10.4043/20659-MS>

Zheng, S. U. (2007), Calculation of Methane Hydrate Solubility in Marine Environment and Its Constraints on Gas Hydrate Occurrence(J),*Chinese Journal of Geophysics* , 50 (5), 1518-1526. <https://doi.org/10.1002/cjg2.1152>

Zhong, J. R., X. Y. Zeng, F. H. Zhou, Q. D. Ran, C. Y. Sun, R. Q. Zhong, L. Y. Yang, G. J. Chen, and C. A. Koh (2016), Self-preservation and structural transition of gas hydrates during dissociation

below the ice point: an in situ study using Raman spectroscopy(J), *Scientific Reports* , 6 (1), 38855.
<https://doi.org/10.1038/srep38855>

MRI insight on natural methane hydrate reservoir system with hydrate, water and gas layers: Development basis of higher-pressure gas reservoir under hydrate layer

Guojun Zhao¹, Huiru Sun¹, Mingjun Yang¹, Jia-nan Zheng^{1,1}, Xin Lv², Yongchen Song^{1,*}

¹ *Key Laboratory of Ocean Energy Utilization and Energy Conservation of Ministry of Education, Dalian University of Technology, Dalian 116024, China*

² *CNOOC Research Institute Co. Ltd, Beijing 100027, China*

Key points:

- First-time experimental visualization on the theoretic sealing effect of natural gas hydrate on its lower gas by MRI.
- Further formation or dissociation of initial formed hydrate under excess water is critical to whether the sealing effect works.
- At least 9.0 MPa pressure difference can exist on both sides of the manmade methane hydrate-containing sealing layer.

Abstract: High-pressure methane gas generally exists stably under methane hydrate stability zone at several hundred meters cutting through the marine sedimentary strata. The usually employed bottom simulating reflector (BSR) for hydrate recognition represents the interface between hydrate and fluid areas in typical natural methane hydrate reservoir system with hydrate, water and gas layers. In this study, the gas-seawater migration in hydrate reservoir was simulated through gas-seawater injection, and the existence of hydrate-containing sealing layer was experimentally confirmed. The hydrate reformation was observed by magnetic resonance imaging (MRI) during the gas-water injection process above the methane hydrate phase equilibrium pressure and it is the fundamental reason that hydrate reservoir has sealing effect on free gas. As the decrease of pore spaces in sediments, the interaction of seawater and hydrate in the reservoir products capillary sealing in the narrow space, thus the free gas and seawater migration are inhibited and the free gas exited stably underlying the hydrate layer. However, low methane concentration in seawater caused by high gas-water flow rate (4–1 ml/min) resulted in the hydrate dissociation, the hydrate-bearing sediments can't produce the sealing effect. Hydrate further forms in the sealing layer and leads to seawater depletion until it is too salty to form hydrate. Finally, the gas layer, water layer and hydrate layer coexist under the seabed. In addition, the hydrate-containing sealing layer could be broken through, and the breakthrough pressure is a significant parameter for hydrate reservoir.

1

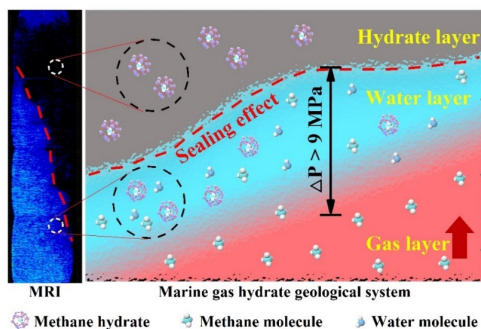
* Corresponding authors.

E-mail addresses: zhengjn@dlut.edu.cn (**J. Zheng**) and songyc@dlut.edu.cn (**Y. Song**).

Keywords Natural hydrate reservoir; Sealing effect; Gas–water flow; MRI

Plain Language Summary

Typical methane hydrate reservoir system in nature generally includes hydrate, water and gas layers, and the already explored marine hydrate reservoir (recognized by bottom simulating reflector method) is just corresponding to this geological reservoir distribution. In marine geology, real gas layer existing stably under the hydrate and water layers may be with higher pressure because of the sealing effect of hydrate layer, and the accurate pressure condition of fully developed gas layer is rarely investigated. We confirm this assumption of natural hydrate and gas reservoirs system accumulation and obtain an entire image of the typical system visually by magnetic resonance imaging. We find that the sealing effect is mainly due to the hydrate reformation and liquid water residue. In order to evaluate the mechanical stability of the sealing effect, we increase the gas pressure to 13 MPa and verify the permitted pressure difference between the two sides of the sealing layer higher than 9.0 MPa. Future geological exploration and joint exploitation project of hydrate and gas reservoirs should refer to these results.



TOC graphic:

1. Introduction

Vast quantities of energy that mankind craves hidden at the bottom of ocean, natural gas hydrate (NGH) is a representative one (Huang *et al.*, 2011). NGH only form under low temperature and high pressure area with sufficient gas and water (Zhong *et al.*, 2016). Seismic reflection method is one the most effective method to detect marine gas hydrate (Tian and Liu, 2020). There are two chief kinds of seismic waves: body waves and surface waves, body waves are mainly used in geological survey. Body waves are divided into longitudinal waves (P waves) and shear waves (S waves). For hydrate in sediments, S waves are more sensitive than P waves, and seismic surveys take the advantage of this acoustic property to detect NGH (Helgerud *et al.*, 2011). The bottom simulating reflector

(BSR) on seismic profile is considered the mark of interface between gas hydrate area and free gas area. Above the BSR, the natural gas exists in hydrate form, and the natural gas exists in the form of free gas below (*Petersen et al.*, 2007). Well logging is another important geophysical method in gas hydrate detect besides seismic reflection, mainly include resistivity log, spontaneous potential log, caliper log, density log and so on (*Ning et al.*, 2013).

According to preliminary statistics, the total amount of stored NGH is approximately $2.1 \times 10^{16} \text{ m}^3$, nearly twice of the traditional fossil fuel (oil and natural gas) reserves in the world, and the total NGH stored in deep sea sediment is up to 99% (*Makogon*, 2010). In the South China Sea, the NGH resourced is up to $(64.35\text{--}77.22) \times 10^9 \text{ t}$ of oil equivalent (*Liu et al.*, 2019), amounting to about half of the total resources of onshore and offshore oil and gas in China (*Shi et al.*, 2019). So far, two NGH production test were carried out in China. In 2017, the China Geological Survey conducted the first production test in Shenhu area (*Li et al.*, 2018). From October 2019 to April 2020, the second offshore NGH production test was conducted in 1225 m deep Shenhu Area (*Liang et al.*, 2020). The success of second production test indicates that safe and effective NGH exploitation is feasible in clayey silt NGH reservoirs (*Qiang et al.*, 2020). Meanwhile, multiple techniques have been tested in Shenhu drilling area. The amplitude behaviors of gas hydrate from stacked seismic data were analyzed, the result shown that free gas zone was accompanied below the gas hydrate zone (*Pibo et al.*, 2017). Through detailed logging data and core analysis from 2020 offshore production test, there was a 24.6 m thick layer consisting of hydrate, free gas and water which was below the hydrate layer (*Qin et al.*, 2020).

Not just in South China Sea, the free gas zone was found stably existed underlain the hydrate reservoir in other areas (*Flemings et al.*, 2003; *Merey and Longinos*, 2018), and it was estimated that the free gas zone may contain from 1/6 to 2/3 of the total methane trapped in hydrate (*Hornbach et al.*, 2004). *Moridis et al.* (2007) also pointed the spatial structure of hydrate reservoir with the free gas and water below the hydrate zone. Recent research had confirmed that in the Hydrate Ridge in offshore Oregon, the hydrate, free gas and seawater coexisted in the hydrate stability zone (*Milkov et al.*, 2004). As for as the Green Canyon in the Gulf in Mexico (*Zhang. and Mcconnell*, 2010) and the Nankai Trough in Japan (*Miyakawa et al.*, 2014). In 1967, the Messoyakha gas field was discovered in Siberia permafrost, the gas zone was enclosed in an anticlinal tectonic circle, and the top of free gas zone was covered with gas hydrate (*Makogon et al.*, 2005). The impermeable boundary was the sedimentary layer which between the gas hydrate zone and the free gas zone (*Collett and Gimsburg*, 1998). Simulation Study shown that the production intervals should be placed far from the impermeable boundary to attain high gas production rates (*Graver et al.*, 2008).

The mechanism of sealing effect for gas hydrate layer is the capillary force between water and hydrate (*Dillon et al.*, 1980; *Su et al.*, 2009). Early in 1999, *Clennell et al.* (1999) systematically analyzed the effect of capillary pressure on

the pore pressure, they explained the pressure of underlying free gas was higher than the theoretical pressure of the formation fluid due to capillary pressure. In recent years, the research of gas hydrates has been gradually developing towards microscopic direction, and the influence of capillary force on gas hydrate has been paid more attention by scholars at home and abroad. Touil et al. (Touil et al., 2019) studied the formation of carbon dioxide hydrate in thin glass tube, the capillary force constrained the direction of hydrate growth, and hydrate grow along the front of the glass wall. Buleiko et al (2017) found the change of propane hydrate formation pressure in porous media using micro calorimeter, because the thermodynamic properties of propane was changed by the capillary effect of pores, which affected propane hydrate.

The large amount of free gas underling the hydrate-containing sealing layer cannot migrate upward because of the sealing effect of hydrate-containing sealing layer (Dillon et al., 1980). Early, natural gas in the deep ocean floor moved upward mainly through diffusion effect (Ming et al., 2017) and solid hydrate is formed in the sedimentary layer that meets the conditions of hydrate formation during this process. Thus, the porosity of the sediments is significantly reduced. The residual water in the narrow pore space of the sedimentary layer creates capillary forces, which pointed down the free gas layer with larger pores volume. Thereby, the hydrate-containing sealing layer is formed to inhibit the upward migration of underlying gas (Xu and Ruppel, 1999).

However, the hydrate-containing sealing layer is not unbreakable. There have been cases of gas leakage under the seabed, such as along the Cascadia continental margin (Heeschen et al., 2005) and offshore Vancouver Island (He et al., 2009). The cold fluids consisting water and hydrocarbon (mostly methane) below the seafloor deposit interface migrate to the seabed by leakage, gushing, or diffusion, this is the cold vent (Logan et al., 2010). The appearance of cold vent is a typical breakthrough of hydrate-containing sealing layer. The gas and seawater generated by breakthrough of hydrate-containing sealing layer will lead to sedimentary layer deformation above the hydrate layer, even cause marine geological disaster (Yang et al., 2020). Therefore, the destruction of hydrate-containing sealing layer must be considered during the hydrate exploitation process.

Although the Marine geology theory has long proposed that hydrate-containing sealing layer is the key for hydrate accumulation, there is no direct experimental evidence of hydrate-containing sealing layer. In this study, the formation process and the existence mode of the hydrate-containing sealing layer were investigated by simulating the process of gas-water migration, the effect of different gas-seawater flow rate and different reservoir pressure on the formation of the hydrate-containing sealing layer was also investigated by MRI. MRI technique was widely used in hydrate investigations because it can distinguish the solid hydrate and liquid water (Song et al., 2015). The research consideration was quit novel, the findings has the significant practical application value to understand the characteristics of hydrate reservoir.

1. Experimental apparatus and procedure

(a) Apparatus

The experimental apparatus is shown in Fig.1. The core device was the MRI system (Varian, Inc Palo Alto, CA, USA), which was used for visualizing methane hydrate formation and dissociation process. And the MRI was operated at 400 MHz with a magnetic field strength of 9.4 Tesla, the standard spin echo pulse to obtain the two-dimensional proton density weighted image. MRI images were constructed by a spin echo multi-slice pulse sequence (SEMS) (Wang *et al.*, 2017), and the experimental parameters were: echo time (TE) 4.39 ms, repetition time (TR) 1000 ms, image data matrix (RO \times RE) 128 \times 128, field of view (FOV) 30 mm \times 30 mm with 2.0 mm thickness. The sequence acquisition time was 2.14 min for per vertical section image and 3.2 min for per cross section image. A high-pressure polyimide tube with a maximum pressure limitation of 13.0 MPa as the reactor had an effective height of 200 mm and diameter of 16 mm. And the reactor was surrounded by a heat preservation jacket in which the coolant circulates continually to keep the tube at required temperature.

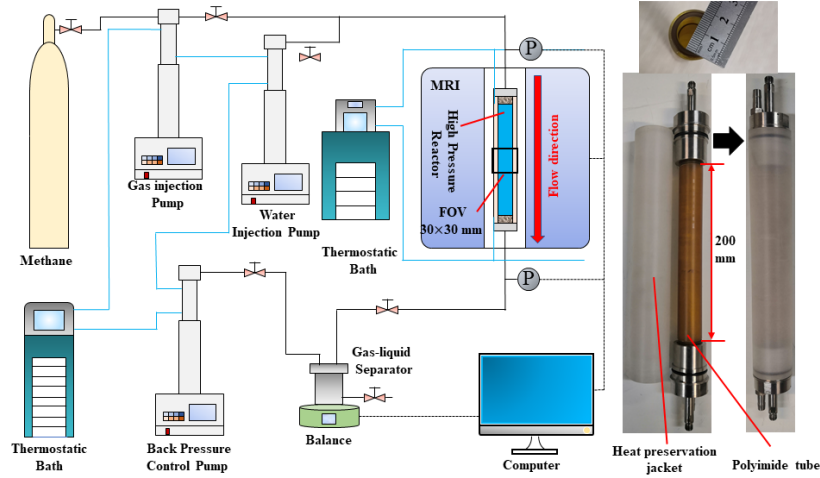


Fig. 1. Schematic of the MRI apparatus.

Three high-precision syringe pumps (260D, Teledyne ISCO Inc, Lincoln, NE, USA) were used in the experiment to inject methane gas and deionized/seawater into the reactor and control the back-pressure of the reactor. Two thermostatic baths (FL300 and FL 25, JULABO, Seelbach, Germany) were used to control the temperature of high precision pump and the reactor. The pressure sensors (3510 CF, Emerson Electric Co., Ltd., St. Louis, USA) with an accuracy of

$\pm 0.05\%$ were connected at the inlet and outlet of the reactor to measure the pressure. According to the results from the core analysis of SHSC-4 (Shenhu area of South China Sea), the mean effective porosity within interval “a” is 35% (Li *et al.*, 2018). Therefore, the glass beads (As-One Co., Ltd., Japan) with a porosity of 35.4% (BZ02) was used to simulate the porous media of marine environment, giving a diameter of 0.177~0.250 mm, so that the maximum of hydrate saturation in theory is higher than 35%. The seawater (deionized water with a salt mass fraction of 3.5%) was used during the flow process, which was more closed to the actual marine environment. In addition, the methane gas with a purity of 99% used in the experiments was produced by Dalian Special Gases Company.

2.2 Procedures

Hydrate sample was made through sand filling, vacuum pumping, water saturation, water displacement and pressurization. Firstly, the glass beads were compacted into the reactor, and the reactor was vacuumed for an hour. Secondly, the outlet valve of the reactor was closed, and the reactor inlet was connected with the water injection pump, the pressure and temperature were constant at 6.0 MPa, 274.15 K, respectively. This was the water saturation process and maintained for about 30 min. Thirdly, closed the water injection pump and opened the reactor outlet value, the reactor pressure dropped to atmosphere. The water in the reactor was displaced to the initial water saturation around 39% using gas injection pump, the initial pressure of gas injection pump is 2.5 MPa. Finally, closed the reactor outlet value and maintained the pressure at 6.0 MPa using gas injection pump, the hydrate formation process began at this point. The entire process was recorded by MRI system and the hydrate saturation (S_h) could be calculated by mean intensity (MI) value through follow equation (Chen *et al.*, 2021):

$$S_h = 1.25 \times \frac{(I_0 - I_i)}{I_0} \times S_{w0} \times 100\% \quad (1)$$

$$S_{w0} = \frac{I_0}{I_{\text{full}}} \quad (2)$$

where I_0 , I_{full} and I_i were MI values of initial water saturation, complete water saturation and water saturation at time i , respectively. S_{w0} represented initial water saturation and can be calculated by equation (2). Additionally, the water saturation at time i (S_{wi}) can be calculated as follow:

$$S_{wi} = \frac{I_i}{I_{\text{full}}} \quad (3)$$

Table 1. Conditions and results of hydrate sample in all cases.

Case	1	2	3	4	5	6	7
Hydrate saturation (%)	35.8	36.9	34.7	34.8	34.3	35.4	34.6
Water saturation (%)	49.2	50.8	52.8	49.8	57.3	54.9	55.8
Pressure (MPa)	6.0						
Temperature (K)	274.15						

The hydrate saturation in hydrate reservoir is usually very high, according to the geological exploration results (*Lpa et al.*, 2019). Thus, when the S_h reached about 35%, opened the outlet valve of the reactor immediately, so the pressure in the reactor was controlled by the back pressure pump, this was the preparation for the gas–seawater flow. At 274.15 K, the phase equilibrium pressure of methane hydrate in seawater was 3.18 MPa (*Lafond et al.*, 2012), the back pressure in this study is 3.5 MPa or 4.0 MPa, which are all above the methane hydrate phase equilibrium pressure. The hydrate reservoir was usually in the state of water saturation (*Almenningen et al.*, 2018; *Chong et al.*, 2017). Therefore, to better simulate the academician state of hydrate in marine environment, the seawater was injected into the reactor using high–precision water injection pump at the flow rate of 0.5 ml/min. The seawater flow rate was low enough so that it can be considered that there was no hydrate decomposition during this process (*Chen et al.*, 2019c). After that, the gas and seawater were injected into the reactor at the same time using pumps. The temperature of injected methane gas and seawater was 273.95 K, which was slightly below the reservoir temperature, for the purpose to avoid the influence of heat injection on hydrate dissociation. The hydrate formation data are shown in Table 1, it was obviously that all experimental conditions were inside the hydrate thermodynamic stable area to avoid the dissociation of hydrate due to other reasons (depressurization, temperature rise).

1. Results and discussion

Methane gas and seawater were injected into the hydrate–bearing sediments to simulate the gas and seawater ascending in the seafloor sediments. Thus, gas–water two phase flow is a method to verify the sealing effect of hydrate reservoir. The water–saturated hydrate samples were made by injecting water into hydrate samples, as shown in Fig. 2. Furthermore, the gas–seawater flow rate ratio was constant at 4 for all Cases. The real–time characteristics of hydrate reservoir state was investigated using MRI visualization technology.

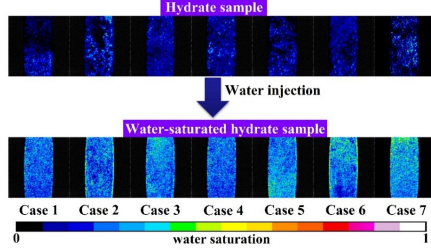


Fig. 2. Initial hydrate reservoir conditions in all cases.

3.1 Methane-containing fluid flow characteristics in hydrate-bearing reservoirs

The free methane gas in the deep ocean floor is bound to migrate upward, and the gas migration also drives the movement of seawater in the sediments (*Su et al.*, 2012). We simulate gas-water migration by injecting gas and water into hydrate-bearing sediments, the experimental conditions of Cases 1–3 are shown in Table 2. The inlet pressure is increasing at the beginning, and large gas-water flow rate makes inlet pressure increase faster, as shown in Fig. 3, because the injection velocity of gas-water is larger than the seepage velocity of hydrate-bearing sediments. In Case 1, the methane gas and seawater were injected into the hydrate-bearing reservoir at the flow rate of 4–1 ml/min. After 52 min, the inlet pressure decreased, and the inlet pressure kept the same with outlet pressure at 136 min, fluids flow through the reservoir smoothly. The outlet flux curve of Case 1 increased and seawater flowed out of the reactor continually, indicating the hydrate reservoir had no sealing effect during gas-water flow process in Case.

Table 2. Experimental conditions and results of Cases 1–3.

Case	Fluid flow conditions	Maximum pressure increase	Hydrate change
1	4 ml/min seawater & 1 ml/min methane	1.76 MPa	dissociation
2	2 ml/min seawater & 0.5 ml/min methane	6.68 MPa	reformation and dissociation
3	1 ml/min seawater & 0.25 ml/min methane	9.50 MPa	reformation

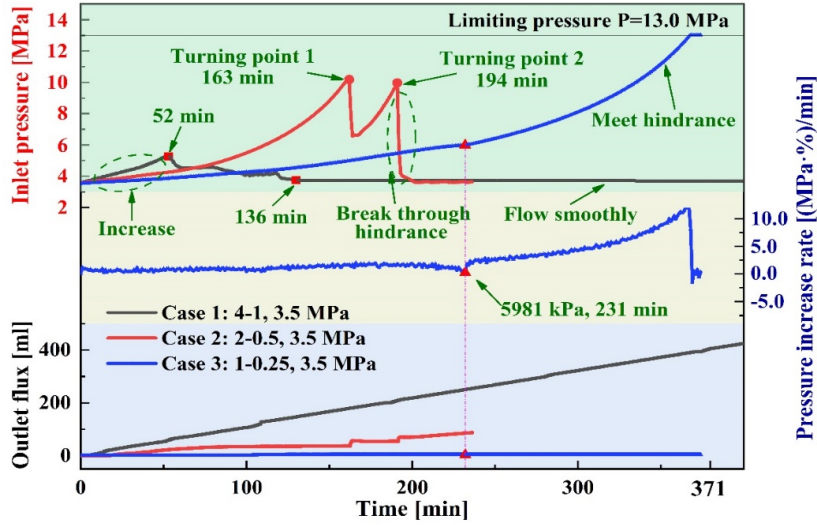


Fig. 3. Characteristics of pressure at reactor inlet and reactor outlet flux

In Case 2, the inlet pressure reached about 10.0 MPa twice at the gas–water flow rate of 2–0.5 ml/min, and finally the inlet pressure dropped the same as outlet pressure. The inlet pressure increased before 163 min (turning point 1), and the seawater accumulated in the reservoir because the slope of outlet flux was decreased gradually. The inlet pressure increase indicating capillary sealing effect (Liu, 2007) appeared in the hydrate reservoir, and the reservoir permeability decreased which was caused by the hydrate saturation increase in the sediments (Mahabadi et al., 2019). But the capillary sealing effect of hydrate reservoir was not stable, the hydrate hydrate saturation was not high enough, the hydrate–containing sealing layer was broken through at 163 and 194 min, respectively, and caused inlet pressure decrease, the whole process is shown in Fig. 4. The break through (BT) pressure were 6.68 MPa, 6.46 MPa, respectively, and the reason of this phenomenon are the large pressure difference on both sides of hydrate reservoir (Liu, 2007) and the incompletely formation of hydrate–containing sealing layer.

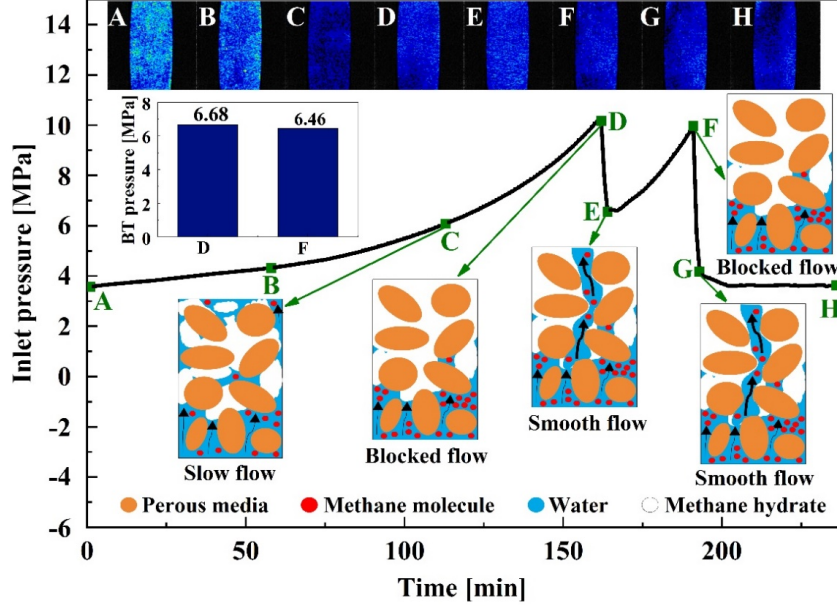


Fig. 4. Breakthrough of hydrate-containing sealing layer in Case 2

In Case 3, the gas-water flow rate was 1–0.25 ml/min. It could be found the inlet pressure kept increasing, so as the pressure difference between reactor inlet and outlet. It was obvious there was a fluctuation in pressure increase rate curve (231 min, and the inlet pressure was 5.98 MPa), and the curve tended to be stable before 231 min, but it got larger after 231 min. After 231 min, the seawater can't flow through the reactor, the hydrate reservoir possessed sealing effect to fluids after 231 min. The pressure increase rate at i min can be calculated by Eq. (4):

$$(4) \quad R_i = \frac{P_i - P_{i+t}}{t} \bullet \%$$

The inlet pressure increased to 13.0 MPa at last, due to the limitation of experimental, thus, at least 9.0 MPa pressure difference existed on both sides of the hydrate reservoir. It's important to emphasize this pressure difference was not caused by gravity, and the sealing effect of hydrate-bearing reservoir, which is shown as pressure difference, represents the ability of hydrate reservoir to trap underlying gas. In addition, this pressure difference providing the development condition of higher-pressure gas reservoir under hydrate layer, and the pressure difference between hydrate zone and gas zone must be considered during hydrate exploitation process.

The reservoir condition could be visually observed by MRI, because the MRI

can only acquire images of the ^1H contained in liquid water (Wang *et al.*, 2020), and the hydrate saturation could be calculated using Eq. (1). Fig. 5(a) shows the characteristics of water distributions in FOV, and Fig. 5(b) reflects the real-time characteristics of hydrate saturation. When the gas-water flow rate was 4-1 ml/min (Case 1), the MRI images brightened gradually after 52 min, and the hydrate saturation decreased, indicating the hydrate dissociated during the gas-water flow process. The reservoir condition (274.15 K, 3.5 MPa) was in hydrate thermodynamic stable area, thus, the driving force for hydrate dissociation was the chemical potential difference between seawater phase and hydrate phase (Chen *et al.*, 2019a; Chen *et al.*, 2019b). The chemical potential difference is caused by the inadequate dissolution of methane gas (Sun *et al.*, 2020b; Zheng, 2007). Hydrate dissociation is the reason that the inlet pressure decreased after 52 min. Thus, hydrate dissociation will reduce or even disappear the sealing effect of hydrate-bearing sediments. For Case 2, the MRI images had no noticeable darkening area, and hydrate saturation curve fluctuated, indicating small amount of hydrate forms. In the gas-water flow rate of 2-0.5 ml/min, hydrates were not always formed or decomposed, it was in an approximate equilibrium state. Thus, the hydrate-containing sealing layer was broken through under large pressure difference. For Case 3, it can be seen that the MRI images going to darken gradually over time, and the hydrate saturation curve presented an increasing trend. Hydrate formed during the gas-water flow process at the flow rate of 1-0.25 ml/min. The inlet pressure was also increased to 13.0 MPa, it could be concluded that hydrate formation enhanced the sealing effect of hydrate-bearing sediments. Hydrate formed continuously even though the sealing effect had been existed in hydrate reservoir. Furthermore, the continuously increasing inlet pressure provided larger driving force for hydrate formation. The hydrate formation before the turning point formed the hydrate-containing sealing layer; the hydrate formation after the turning point further enhanced the hydrate-containing sealing layer. After the turning point (231 min), the seawater can't flow through the reactor, indicating the reservoir had sealing effect. The mechanism of sealing effect is because that the sediment pores were occupied by more hydrate and became smaller, the residual water in the sediment created capillary forces in the narrow pore space, which blocked the gas-water migration.

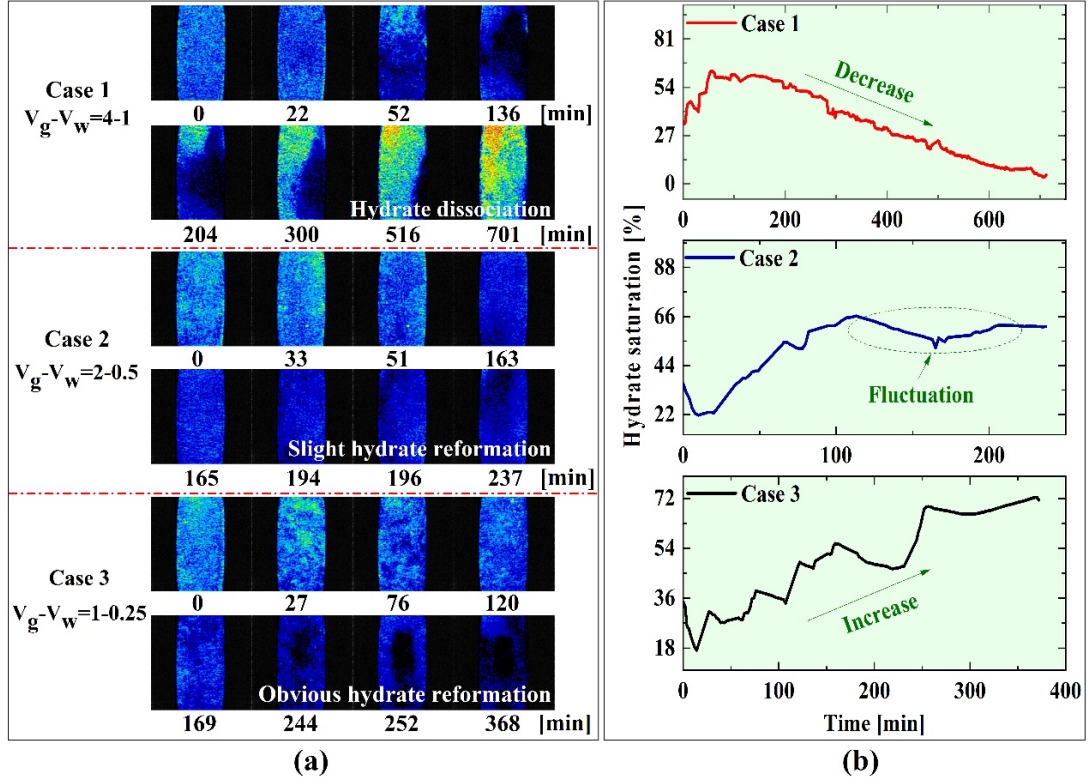


Fig. 5. Micro-images during the gas-seawater flow process in Cases 1-3: (a) MRI images; (b) hydrate saturation

In conclusion, the hydrate-containing sealing layer formed when the gas-water flow rate is 1-0.25 ml/min. The seawater is full contact with the methane gas in lower gas-water flow rate, methane saturation in seawater is high enough to induce the hydrate reformation. The decrease of pore volume leads to the increase of capillary force, thus, sealing layer formed, this is the formation mechanism of hydrate-containing sealing layer. Then, the hydrate continued to form in the reservoir which enhanced the sealing layer and makes it more difficult to be destroyed.

3.2 Sealing characteristics of hydrate-bearing reservoir on external fluids

Hydrate reformation is the reason that sealing effect exists in hydrate-bearing sediments. We increased the hydrate formation rate by increasing reservoir pressure to 4.0 MPa, the characteristics of hydrate-containing sealing layer was investigated, the experimental conditions of Cases 4 and 5 are shown in Table 3. Take the injection volume as the reference value, it was found that high flow

rate (Case 5) has hysteresis phenomenon compared with low flow rate (Case 4), but higher flow rate consumed less time.

Table 3. Experimental conditions and results of Cases 4 and 5.

Case	Fluid flow conditions	Maximum pressure increase	Hydrate change	Final flo
4	2 ml/min seawater & 0.5 ml/min methane	9.00 MPa	reformation	hindered
5	4 ml/min seawater & 1 ml/min methane	9.00 MPa	reformation	hindered

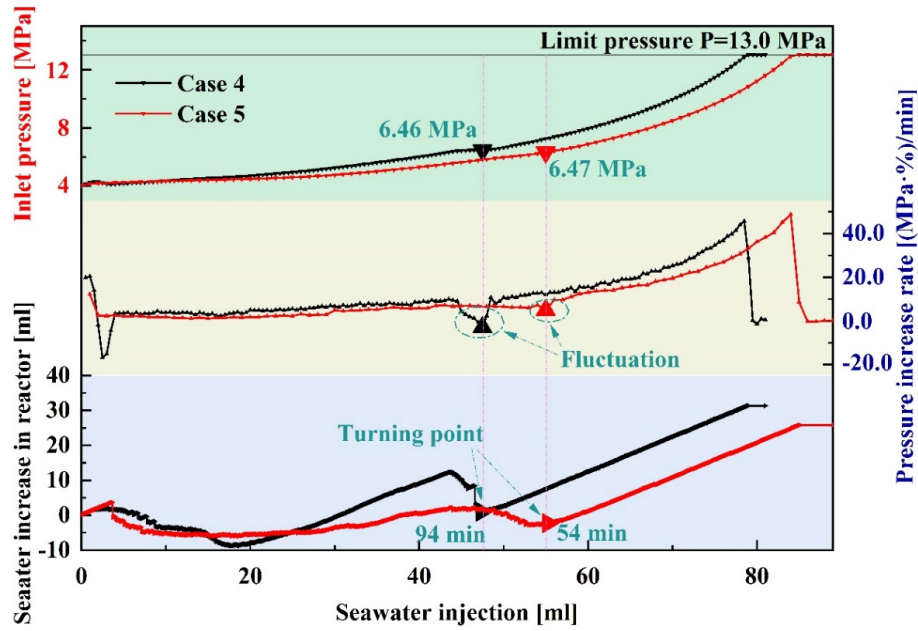


Fig. 6. Characteristics of pressure at reactor inlet and seawater increase in reactor

As shown in Fig. 6, the turning points appeared at 94 and 54 min in Cases 4 and 5, respectively. After the turning point, the seawater won't flow out of the reservoir outlet, the hydrate reservoir had sealing effect. The gas-water flow rates of Cases 4 and 5 were the same as Cases 2 and 1, respectively. However, hydrate-containing sealing layer formed only in Cases 4 and 5, because higher reservoir pressure provide larger driving force for hydrate formation (*Ma et al.*, 2020). It also indicated that higher pressure will promote the formation of hydrate-containing sealing layer than low gas-water flow rate. Because the higher pressure can enhance the mass transfer between the gas and seawater, and enhance hydrate formation during gas-water flow process. Moreover, the pressure increases rate curve had a fluctuation at the turning point, and increase

rate of inlet pressure was decreased, this fluctuation also appeared in Case 3. Furthermore, there is a certain regularity in the pressure difference between the reactor inlet and outlet at the time of hydrate-containing sealing layer is formal formed, as shown in Fig. 7. The mean value of pressure different is 2.47 MPa. In this study, the pressure difference at turning point is independent of reservoir pressure, it can be used as a marker to judge the formation of hydrate seal layer during the experiment.

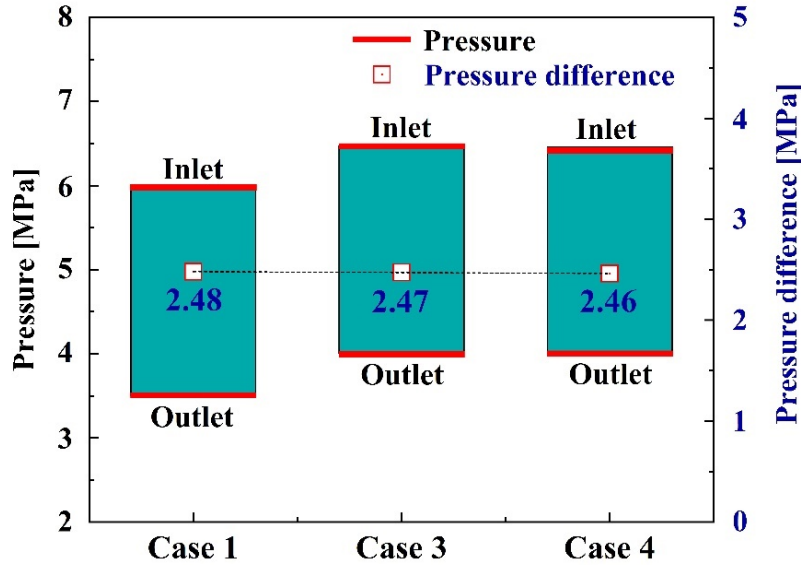


Fig. 7. Pressure difference values at onset time of sealing layer formation

Fig. 8 shows the variation characteristics of hydrate saturation in FOV during the gas-water injection process of cases 4 and 5. The MRI images is getting darker in Case 5 and hydrate saturation present an increasing trend, thus, hydrate formed during the gas-water flow process and hydrate-bearing reservoir had sealing effect. However, hydrate saturation didn't show an obviously increasing trend in Case 4, though the sealing effect existed after 94 min. It could be found that there was a significant change in the lower left corner of FOV in Case 4, so we analyzed the change in MI value of Line 1. The small distance of MI value (0~4.2 mm) is obviously reduced, indicating that hydrate formed in this area and consumed the pore water. The reason for sealing effect exists in Case 4 was also caused by hydrate formation, but hydrate formation was not concentrated in the FOV, and thought it was below the FOV. To further analyze the reservoir state, multi-level MRI image (4 layers) was carried out by adjusting the position of the reactor.

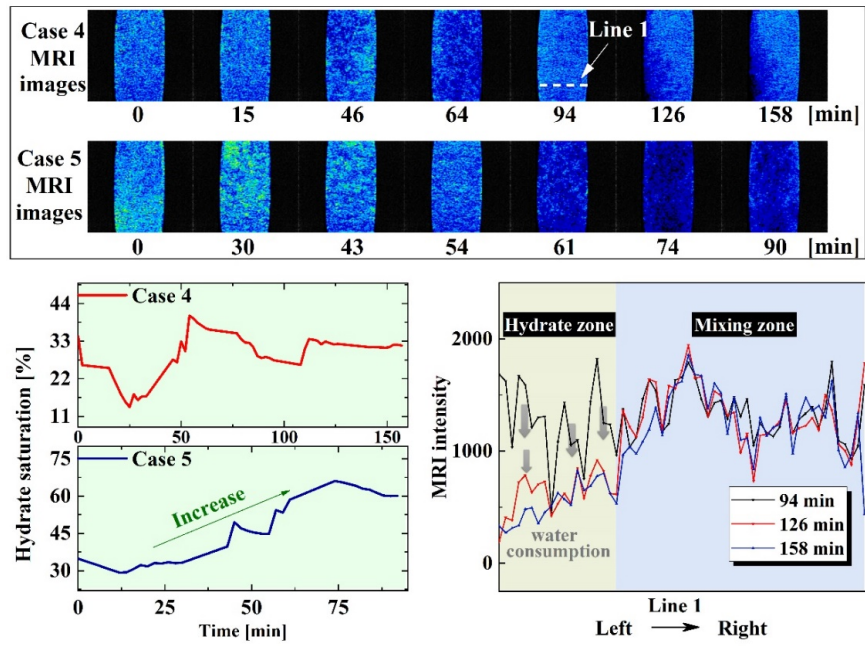


Fig. 8. Main results of Cases 4 and 5

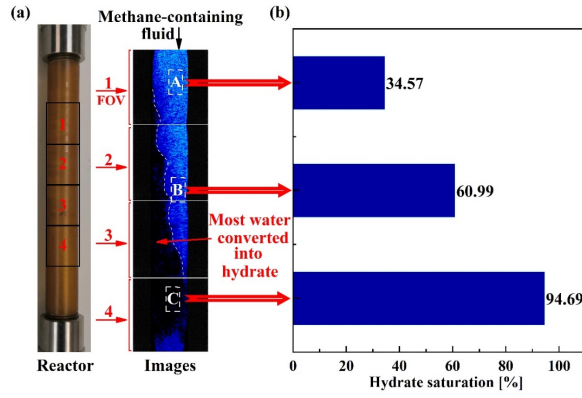


Fig. 9. (a) multi-level MRI images in Case 4; (b) hydrate saturation in different areas

Fig. 9(a) was the multi-level MRI images of reactor after 158 min in Case 4. The camera on the MRI device remained stationary, and moved the reactor 30 mm upwards after each shot, for the reason the FOV was 30 mm \times 30 mm, complete reservoir status is presented by this operation. The gas-water injection was stopped and the inlet pressure was constant at 13.0 MPa during the whole shooting process. Significant brightness differences could be found in the hydrate reservoir. By comparing the hydrate saturation in different areas, as shown in Fig. 9(b), the hydrate saturation was higher in farther area along the gas-water injection direction. The pore seawater in area C was almost consumed up, tiny amount of seawater still remained in the hydrate reservoir and it is too saline to form hydrate, it was hydrate zone. The brighter area (areas A and B) compared with area C was water zone (seawater, hydrate, gas coexisted). The free gas was hindered out of the reactor inlet. Thus, the hydrate reservoir can be divided into three layers. This is very similar to the hydrate reservoir with three structures in the South China Sea: gas hydrate layer; mixing layer consisting of hydrates, free gas and seawater; free gas layer coexists from top to bottom (Qin *et al.*, 2020). And the experimental phenomenon is consistent with the model for free gas migration presented by Liu *et al* (Liu and Flemings, 2006).

3.3 Effects of hydrate saturation change on the sealing layer formation process

In Cases 3, 4, 5, the inlet pressure increased as soon as the gas-water flowed, indicating the hydrate-containing sealing layer formed at the beginning. Thus, we investigated the effects of hydrate saturation change on sealing layer by

increasing seawater injection rate ratio, the experimental conditions of Cases 6 and 7 are shown in Table 4. When seawater flow in hydrate reservoir was enhanced, the reservoir won't produce sealing effect during flow process. The gas-water process was divided into two stages (see Fig. 10): in the first stages the gas-water flow rate was 1–2 ml/min, in the second stage, the gas-water flow rate was 2–0.5 ml/min in Case 5 and 4–1 ml/min in Case 6, respectively.

Table 4. Experimental conditions and results of Cases 6 and 7.

Case	Fluid flow conditions in step 1	Fluid flow conditions in step 2	Hydrate change
6	1 ml/min seawater & 2 ml/min methane	2 ml/min seawater & 0.5 ml/min methane	dissociation in
7	1 ml/min seawater & 2 ml/min methane	4 ml/min seawater & 1 ml/min methane	dissociation in

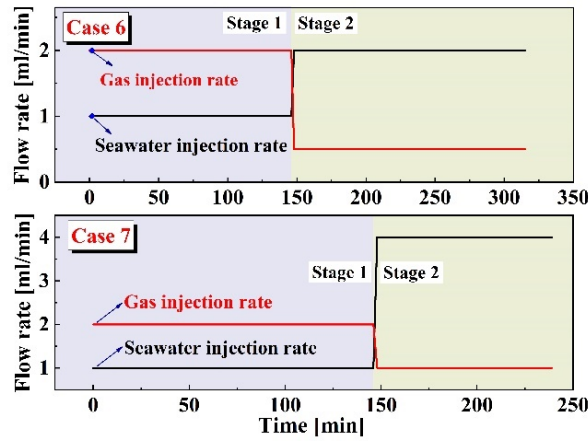


Fig. 10. Gas-water injection rates in Case 6 and Case 7

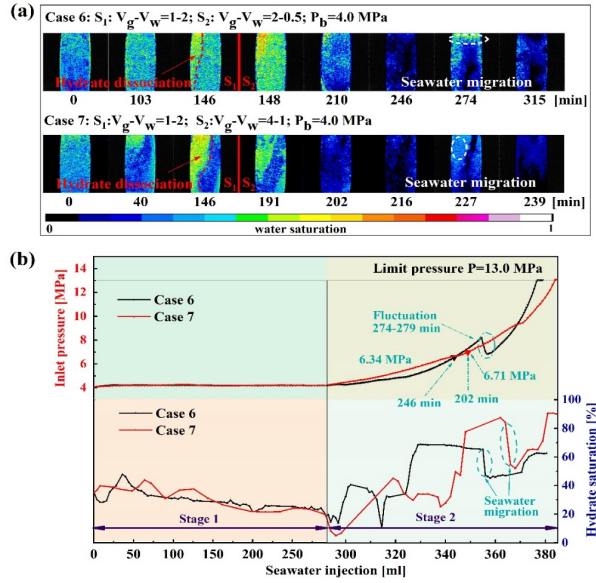


Fig. 11. MRI images and inlet pressure and hydrate saturation changes in Cases 6 and 7

Fig. 11 shows MRI images in FOV and the characteristics of hydrate saturation during the whole flow process. In the stage 1 (S_1), the inlet pressure of both cases remained stable around 4.0 MPa. However, the inlet pressure is slightly higher than the back pressure (about 4.2 MPa), because the contact of seawater and hydrate causes the capillary force in the sediments. The MRI images of S_1 brightened, indicating the hydrate dissociated during the gas–water flow process with the flow rate of 1–2 ml/min. Because the large amounts of seawater flow enhanced the mass transfer between hydrate phase and seawater phase, the driving force is the chemical potential difference caused by low methane concentration in seawater (Sun *et al.*, 2020a; Yang *et al.*, 2019). Meanwhile, the random distribution of hydrate in porous media was the reason that the seawater–hydrate interface in Case 6 and Case 7 was different (Zhang *et al.*, 2019). The hydrate dissociation areas in Fig. 11(a) could be considered the chimney in the hydrate reservoir (Torres *et al.*, 2004), the reservoir had no sealing effect and showed well permeability characteristics.

In the stage 2, the gas–water flow in hydrate–bearing sediments with chimney due to hydrate dissociation in stage 1, it was obvious that the reactor inlet pressure was increasing, shown in Fig. 11(b), and the corresponding MRI images went dimmed, hydrate saturation increased. As the seawater flow rate decreased and methane gas flow rate increased, the methane dissolved more fully in seawater. Thus, the hydrate formed inside the hydrate thermodynamically stable area, the gas–water flow process in S_2 was the formation process of hydrate–

containing sealing layer. In Case 6, no more seawater flowed out of the reactor after 246 min, hydrate-containing sealing layer had sealing effect at this moment. The inlet pressure fluctuated in 274~279 min, and seawater flowed into the FOV. Under the driving of pressure difference, the hydrate-containing sealing layer was partially destroyed and seawater migrated in the reservoir, but the seawater did not break through the sealing layer. The hydrate continuously formed after 279 min, the pore volume is reduced, thus the inlet pressure increased faster. In Case 6, the turning point appeared at 202 min, the pressure difference of in and out is 2.34 MPa in Case 5 and 2.71 MPa in Case 6, respectively. They were all close to the mean value of pressure different (2.47 MPa), the pressure difference of in and out could be a marker to judge the formation of hydrate-containing sealing layer. In hydrate-bearing sediments, the hydrate-containing sealing layer can be formed when hydrate reforms in hydrate reservoir, even though hydrate has dissociated before.

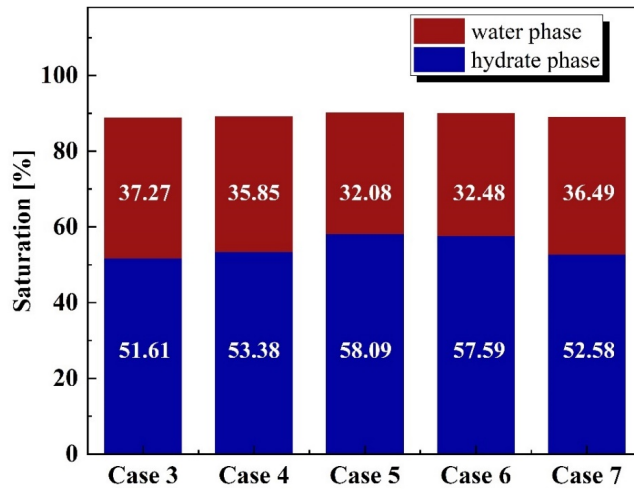


Fig. 12. Saturations of hydrate and water phases below hydrate zone at sealing onset in different cases.

The hydrate-containing sealing layer formed in cases 3, 4, 5, 6, 7 for the reason that hydrate reformed in hydrate-bearing sediments. Hydrate saturation is the most direct criterion to judge whether hydrate reservoir has sealing effect. Seawater is almost consumed up of Area A in Fig. 9(a) and hydrate saturation is close to 100%, thus, we choose Area B in Fig. 9(a) as reference. Hydrate saturation at the turning point for cases 3, 4, 5, 6, 7 are shown in Fig. 12. It is obvious that hydrate saturation is above 51.61%, we consider this is the lowest hydrate saturation that reservoir has sealing effect, and the water saturation is

between 32.08% and 37.27%. If the hydrate saturation is higher than 37.27%, sealing effect of hydrate-containing sealing layer may not exist due to insufficient conversion of water to hydrate, and the water saturation will decrease as the hydrate continues to form in hydrate-containing sealing layer.

1. Conclusion

In this study, the existence of hydrate-containing sealing layer is firstly experimentally confirmed using MRI visualization device by injecting methane gas and seawater into hydrate reservoirs at 3.5 and 4.0 MPa and 274.15 K. The reformation of hydrates at low gas-water flow rate or high reservoir pressure environment (hydrate saturation is higher than 51.61%) is confirmed contributed to the occurrence of sealing effect that hinders the external fluids flowing through the reservoir. Near all of pore water has been consumed to form hydrates in the sealing layer. In addition, the same pressure difference of approximately 2.47 MPa between reactor inlet and outlet was found in the different experimental cases that process sealing layers and could be a significant marker suitable for hydrate reformation. This is also a novel method, put forward in this study, to form hydrate-containing sealing layer in experimental condition. When the hydrates dissociate by high-rate gas-water flow, the sealing effect does not exist any longer. The entire natural gas hydrate reservoir, which includes three-layer distribution of hydrate, water, and gas from top to bottom, recognized by BSR is perfectly demonstrated by MRI images in this study, and A pressure difference of at least 9.0 MPa is found existing on both sides of the sealing layer, providing the development condition of higher-pressure gas reservoir under hydrate layer. The results of this study reveal the key reason why free gas can exist stably underling hydrate layer in nature and can guide the safe joint exploitation of hydrate and gas reservoirs.

Acknowledgments

This project was financially supported by the National Natural Science Foundation of China (51822603, U19B2005), Liao Ning Revitalization Talents Program (XLYC1907096), the Innovation Foundation of Science and Technology of Dalian (2019J11CY012) and the Fundamental Research Funds for the Central Universities of China (DUT21ZD103).

Declaration of Competing Interest

The authors declare that they have no known competing financial interests or personal relationships that could have appeared to influence the work reported in this paper.

CRedit authorship contribution statement

Guojun Zhao: Methodology, Visualization, Writing original draft, Writing review & editing. **Huiru Sun:** Data curation. **Mingjun Yang:** Formal analysis, Supervision. **Jia-nan Zheng:** Conceptualization, Investigation. **Xin Lv:** Resources. **Yongchen Song:** Supervision.

References

- Almenningen, S., J. Gauteplass, P. Fotland, G. L. Aastveit, T. Barth, and G. Ersland (2018), Visualization of hydrate formation during CO₂ storage in water-saturated sandstone(J), *International Journal of Greenhouse Gas Control*, 119, 678-687. <https://doi.org/10.1016/j.ijggc.2018.11.008>
- Buleiko, V. M., B. A. Grigoriev, and V. A. Istomin (2017), Capillary effects on phase behavior of liquid and gaseous propane and dynamics of hydrate formation and dissociation in porous media, *Fluid Phase Equilib.*, 441, 64-71, doi:10.1016/j.fluid.2017.01.026. <https://doi.org/10.1016/j.fluid.2017.01.026>
- Chen, Z. Liu, H. Sun, G. Zhao, and M. Yang (2021), The synthetic effect of traditional-thermodynamic-factors (temperature, salinity, pressure) and fluid flow on natural gas hydrate recovery behaviors(J), *Energy*(1), 121147. <https://doi.org/10.1016/j.energy.2021.121147>
- Chen, H. Sun, K. Li, D. Wang, and M. Yang (2019a), Experimental investigation of natural gas hydrate production characteristics via novel combination modes of depressurization with water flow erosion(J), *Fuel*, 252, 295-303. <https://doi.org/10.1016/j.fuel.2019.04.120>
- Chen, H. Sun, H. Zhou, M. Yang, and D. Wang (2019b), Effects of pressure and sea water flow on natural gas hydrate production characteristics in marine sediment(J), *Applied Energy*, 238(MAR.15), 274-283. <https://doi.org/10.1016/j.apenergy.2019.01.095>
- Chen, M. Yang, H. Sun, P. Wang, and D. Wang (2019c), Visualization study on the promotion of natural gas hydrate production by water flow erosion(J), *Fuel*, 235(JAN.1), 63-71. <https://doi.org/10.1016/j.egypro.2019.01.586>
- Chong, Z. R., Z. Yin, J. Tan, and P. Linga (2017), Experimental investigations on energy recovery from water-saturated hydrate bearing sediments via depressurization approach(J), *Applied Energy*, 204, 1513-1525. <https://doi.org/10.1016/j.apenergy.2017.04.031>
- Clennell, M. B., P. Henry, M. Hovland, J. S. Booth, and M. Thomas (1999), Formation of natural gas hydrates in marine sediments: 1. Conceptual model of gas hydrate growth conditioned by host sediment properties(J), *Annals of the New York Academy of Sciences*, 104(1), 22985-23003. <https://doi.org/10.1029/1999JB900175>
- Collett, T. S., and G. D. Ginsburg (1998), Gas Hydrates In the Messoyakha Gas Field of the West Siberian Basin - A Re-Examination of the Geologic Evidence(J), *International Journal of Offshore & Polar Engineering*, 8(1), 22-29. Paper Number: ISOPE-98-08-1-022
- Dillon, W. P., J. A. Grow, and C. K. Paull (1980), Unconventional gas hydrate seals may trap gas off southeast U.S(J), *Oil and Gas Journal*, 78(1), 124-130. [https://doi.org/10.1016/S0025-3227\(99\)00128-0](https://doi.org/10.1016/S0025-3227(99)00128-0)

- Flemings, P. B., X. Liu, and W. J. Winters (2003), Critical pressure and multiphase flow in Blake Ridge gas hydrates(J), *Geology*, *31*(12), 1057-1060. <https://doi.org/10.1130/G19863.1>
- Graver, T., G. Moridis, and S. A. Holditch (2008), Analysis of Reservoir Performance of Messoyakha Gas Hydrate Field(D), Proceedings of the International Offshore and Polar Engineering Conference.
- He, T., G. D. Spence, W. T. Wood, M. Riedel, and R. D. Hyndman (2009), Imaging a hydrate-related cold vent offshore Vancouver Island from deep-towed multichannel seismic data(J), *Geophysics*, *74*(2), B23. <https://doi.org/>
- Heeschen, K. U., R. W. Collier, M. Angelis, E. Suess, G. Rehder, P. Linke, and G. P. Klinkhammer (2005), Methane sources, distributions, and fluxes from cold vent sites at Hydrate Ridge, Cascadia Margin(J), *Global Biogeochemical Cycles*, *19*. <https://doi.org/10.1029/2004GB002266>
- Helgerud, M. B., W. F. Waite, S. H. Kirby, and A. Nur (2011), Measured temperature and pressure dependence of V-p and V-s in compacted, polycrystalline sI methane and sII methane-ethane hydrate(J), *Canadian Journal of Physics*, *81*(1-2), 47-53. <https://doi.org/10.1139/P03-016>
- Hornbach, M. J., D. M. Saffer, and W. S. Holbrook (2004), Critically pressured free-gas reservoirs below gas-hydrate provinces(J), *Nature*, *427*(6970), 142-144. <https://doi.org/10.1038/nature02172>
- Huang, B. X., W. C. Xue, Y. Z. Wang, and T. Zhang (2011), Review of Theory and Practice on Natural Gas Hydrate(J), *Advanced Materials Research*, *361-363*, 149-160. <https://doi.org/10.4028/AMR.361-363.149>
- Lafond, P. G., K. A. Olcott, E. D. Sloan, C. A. Koh, and A. K. Sum (2012), Measurements of methane hydrate equilibrium in systems inhibited with NaCl and methanol(J), *Journal of Chemical Thermodynamics*, *48*, 1-6. <https://doi.org/10.1016/j.jct.2011.12.023>
- Li, J., et al. (2018), The first offshore natural gas hydrate production test in South China Sea(J), *China Geology*, *1*(1), 5-16, doi:10.31035/cg2018003. <https://doi.org/10.31035/cg2018003>
- Liang, J. Q., W. Deng, J. A. Lu, Z. G. Kuang, and M. M. Meng (2020), A fast identification method based on the typical geophysical differences between submarine shallow carbonates and hydrate bearing sediments in the northern South China Sea(J), *China Geology*, *3*(1), 16-27. <https://doi.org/10.31035/cg2020021>
- Liu (2007), Dynamic multiphase flow model of hydrate formation in marine sediments(J), *Journal of Geophysical Research Solid Earth*, *112*(B3), B03101. <https://doi.org/10.1029/2005JB004227>
- Liu, and P. B. Flemings (2006), Passing gas through the hydrate stability zone at southern Hydrate Ridge, offshore Oregon(J), *Earth & Planetary Science Letters*, *241*(1-2), 211-226. <https://doi.org/10.1016/j.epsl.2005.10.026>

- Liu, Liping, SUN, Zhilei, ZHANG, Lei, WU, Nengyou, Yichao, and Qin (2019), Progress in Global Gas Hydrate Development and Production as a New Energy Resource(J), *Acta Geologica Sinica(English Edition)*, v.93(03), 231-255. <https://doi.org/10.1111/1755-6724.13876>
- Logan, G. A., A. T. Jones, J. M. Kennard, G. J. Ryan, and N. Rollet (2010), Australian offshore natural hydrocarbon seepage studies, a review and re-evaluation(J), *Marine & Petroleum Geology*, 27(1), 26-45. <https://doi.org/10.1016/j.marpetgeo.2009.07.002>
- Lpa, B., B. Ksa, and A. Akj (2019), Estimate of gas hydrate saturations in the Krishna-Godavari basin, eastern continental margin of India, results of expedition NGHP-02(J), *Marine and Petroleum Geology*, 108, 581-594. <https://doi.org/10.1016/j.marpetgeo.2018.12.009>
- Ma, S., J. N. Zheng, M. Tian, D. Tang, and M. Yang (2020), NMR quantitative investigation on methane hydrate formation characteristics under different driving forces(J), *Fuel*, 261(Feb.1), 116361-116364. <https://doi.org/10.1016/j.fuel.2019.116364>
- Mahabadi, N., S. Dai, Y. Seol, and J. Jang (2019), Impact of hydrate saturation on water permeability in hydrate-bearing sediments(J), *Journal of Petroleum Science and Engineering*, 174, 696-703. <https://doi.org/10.1016/j.petrol.2018.11.084>
- Makogon (2010), Natural gas hydrates – A promising source of energy(J), *Journal of Natural Gas Science and Engineering*, 2(1), 49-59. <https://doi.org/10.1016/j.jngse.2009.12.004>
- Makogon, S. A. Holditch, and T. Y. Makogon (2005), Russian field illustrates gas-hydrate production(J), *Oil and Gas Journal*, 103(5), 43-47. <https://doi.org/WOS:000226889700015>
- Merey, ü., and S. N. Longinos (2018), Numerical simulations of gas production from Class 1 hydrate and Class 3 hydrate in the Nile Delta of the Mediterranean Sea(J), *Journal of Natural Gas Science and Engineering*, 52, 248-266. <https://doi.org/10.1016/j.jngse.2018.01.001>
- Milkov, A. V., G. R. Dickens, G. E. Claypool, Y. J. Lee, W. S. Borowski, M. E. Torres, W. Xu, H. Tomaru, A. Tréhu, and P. Schultheiss (2004), Co-existence of gas hydrate, free gas, and brine within the regional gas hydrate stability zone at Hydrate Ridge (Oregon margin): evidence from prolonged degassing of a pressurized core(J), *Earth & Planetary Science Letters*, 222(3-4), 829-843. <https://doi.org/10.1016/j.epsl.2004.03.028>
- Ming, S., S. Zhibin, Z. Cuimei, W. Hongbin, W. Nengyou, Y. Rui, L. Jinqiang, Q. Shaohua, C. Xiaorong, and L. Jie (2017), Types, characteristics and significances of migrating pathways of gas-bearing fluids in the Shenhu area, northern continental slope of the South China Sea, *Acta Geol. Sin.-Engl. Ed.*, 91(1), 219-231. <https://doi.org/10.1111/1755-6724.13073>

- Miyakawa, A., S. Saito, Y. Yamada, H. Tomaru, M. Kinoshita, and T. Tsuji (2014), Gas hydrate saturation at Site C0002, IODP Expeditions 314 and 315, in the Kumano Basin, Nankai trough(J), *Island Arc*, 23(2), 142-156. <https://doi.org/10.1111/iar.12064>
- Moridis, G. J., M. B. Kowalsky, and K. Pruess (2007), Depressurization-Induced Gas Production From Class-1 Hydrate Deposits(J), *Society of Petroleum Engineers Reservoir Evaluation Andengineering*, 10(05), 458-481. <https://doi.org/10.2118/97266-PA>
- Ning, F., N. Wu, S. Li, K. Zhang, Y. Yu, L. Liu, J. Sun, G. Jiang, C. Sun, and G. Chen (2013), Estimation of in-situ mechanical properties of gas hydrate-bearing sediments from well logging(J), *Petroleum Exploration & Development*, 40(4), 542-547. <https://doi.org/> [https://doi.org/10.1016/S1876-3804\(13\)60071-3](https://doi.org/10.1016/S1876-3804(13)60071-3)
- Petersen, C. J., C. Papenberg, and D. Klaeschen (2007), Local seismic quantification of gas hydrates and BSR characterization from multi-frequency OBS data at northern Hydrate Ridge(J), *Earth and Planetary Science Letters*, 255(3), 414-431. <https://doi.org/10.1016/j.epsl.2007.01.002>
- Pibo, S. U., J. Liang, Z. Zhang, and Z. Sha (2017), Analysis on the bright spots and dim out of seismic section for diffusion-type hydrate in Shenhu area(J), *Earth Science Frontiers*, 04, 57-62. <https://doi.org/CSCD:6018712>
- Qiang, C., G. W. Hu, N. Y. Wu, C. L. Liu, Q. G. Meng, C. F. Li, J. Y. Sun, and Y. L. Li (2020), Evaluation of clayed silt properties on the behavior of hydrate production in South China Sea(J), *China Geology*, 3(3), 362-368. <https://doi.org/10.31035/cg2020050>
- Qin, X. W., J. A. Lu, H. L. Lu, H. J. Qiu, J. Q. Liang, D. J. Kang, L. S. Zhan, H. F. Lu, and Z. G. Kuang (2020), Coexistence of natural gas hydrate, free gas and water in the gas hydrate system in the Shenhu Area, South China Sea(J), *China Geology*, 3(2), 210-220. <https://doi.org/10.31035/cg2020038>
- Shi, Y., Q. Liang, J. Yang, Q. Yuan, X. Wu, and L. Kong (2019), Stability analysis of submarine slopes in the area of the test production of gas hydrate in the South China Sea(J), *China Geology*, 2(3), 274-284, doi:10.31035/cg2018122. <https://doi.org/10.31035/cg2018122>
- Song, Y., P. Wang, L. Jiang, Y. Zhao, and M. Yang (2015), Methane hydrate formation/reformation in three experimental modes: A preliminary investigation of blockage prevention during exploitation(J), *Journal of Natural Gas Science & Engineering*, 27, 1814-1820. <https://doi.org/10.1016/j.jngse.2015.11.009>
- Su, Z., Y. Cao, N. Wu, D. Chen, S. Yang, and H. Wang (2012), Numerical investigation on methane hydrate accumulation in Shenhu Area, northern continental slope of South China Sea(J), *Marine & Petroleum Geology*, 38(1), 158-165. <https://doi.org/10.1016/j.marpetgeo.2012.06.005>
- Su, Z., Y. C. Cao, N. Y. Wu, L. M. Cathles, and D. F. Chen (2009), Numerical computation and case analysis of the venting process of free gas

- beneath hydrate layer(J), *Chinese Journal of Geophysics*, 52(12), 3124-3131. <https://doi.org/10.3969/j.issn.0001-5733.2009.12.022>
- Sun, H., B. Chen, and M. Yang (2020a), Effect of multiphase flow on natural gas hydrate production in marine sediment(J), *Journal of Natural Gas Science and Engineering*, 73, doi:10.1016/j.jngse.2019.103066. <https://doi.org/10.1016/j.jngse.2019.103066>
- Sun, H., B. Chen, G. Zhao, Y. Zhao, and M. Yang (2020b), Utilization of water-gas flow on natural gas hydrate recovery with different depressurization modes(J), *Fuel*, doi:10.1016/j.fuel.2020.119583. <https://doi.org/10.1016/j.fuel.2020.119583>
- Tian, D., and X. Liu (2020), A new approach for the identification of gas hydrate in marine sediments(J), *Marine Geophysical Research*, 41(3), 1-12. <https://doi.org/10.1007/s11001-020-09412-y>
- Torres, M. E., K. Wallmann, A. Tréhu, G. Bohrmann, W. S. Borowski, and H. Tomaru (2004), Gas hydrate growth, methane transport, and chloride enrichment at the southern summit of Hydrate Ridge, Cascadia margin off Oregon(J), *Earth and Planetary Science Letters*, 226(1-2), 225-241. <https://doi.org/10.1016/j.epsl.2005.05.044>
- Touil, A., D. Broseta, and A. Desmedt (2019), Gas hydrate crystallization in thin glass capillaries: Roles of supercooling and wettability, *Langmuir*, 35(38), 12569-12581. <https://doi.org/10.1021/acs.langmuir.9b01146>
- Wang, Y. Liu, Y. Zhao, Y. Zhang, and Y. Song (2020), Enhanced Mass Transfer by Density-Driven Convection during CO₂ Geological Storage, *Industrial & Engineering Chemistry Research*, 59(19), 9300-9309. <https://doi.org/10.1021/acs.iecr.0c00525>
- Wang, S. Wang, Y. Song, and M. Yang (2017), Methane Hydrate Formation and Decomposition Properties During Gas Migration in Porous Medium(J), *Energy Procedia*, 105, 4668-4673. <https://doi.org/10.1016/j.egypro.2017.03.1012>
- Xu, W., and C. Ruppel (1999), Predicting the occurrence, distribution, and evolution of methane gas hydrate in porous marine sediments(J), *Journal of Geophysical Research Solid Earth*, 104(B3), 5081-5096. <https://doi.org/10.1029/1998JB900092>
- Yang, H. Sun, B. Chen, and Y. Song (2019), Effects of water-gas two-phase flow on methane hydrate dissociation in porous media(J), *Fuel*, 255, doi:10.1016/j.fuel.2019.115637. <https://doi.org/10.1016/j.fuel.2019.115637>
- Yang, J. Wang, and Y. Jiang (2020), Experimental Study and Numerical Simulation of Overlying Layer Soil Failure Caused by Hydrate Decomposition(J), *ACS Omega*, 5(48), 31244-31253. <https://doi.org/10.1021/acsomega.0c04619>
- Zhang, L., L. Sun, M. Sun, X. Lv, and J. Zhao (2019), Analyzing spatially and temporally visualized formation behavior of methane hydrate in un-

consolidated porous media(J), *Magnetic Resonance Imaging*, 61, 224-230. <https://doi.org/10.1016/j.mri.2019.06.005>

Zhang., and D. R. McConnell (2010), Seismic Modeling Analysis and Characterization of a Gas Hydrate and Free Gas Mixed System in Green Canyon, Gulf of Mexico(J), *Proceedings of the Annual Offshore Technology Conference*, 2, 1530-1541. <https://doi.org/10.4043/20659-MS>

Zheng, S. U. (2007), Calculation of Methane Hydrate Solubility in Marine Environment and Its Constraints on Gas Hydrate Occurrence(J), *Chinese Journal of Geophysics*, 50(5), 1518-1526. <https://doi.org/10.1002/cjg2.1152>

Zhong, J. R., X. Y. Zeng, F. H. Zhou, Q. D. Ran, C. Y. Sun, R. Q. Zhong, L. Y. Yang, G. J. Chen, and C. A. Koh (2016), Self-preservation and structural transition of gas hydrates during dissociation below the ice point: an in situ study using Raman spectroscopy(J), *Scientific Reports*, 6(1), 38855. <https://doi.org/10.1038/srep38855>